Climatic and environmental changes across the Early Eocene Climatic Optimum at mid-Waipara River, Canterbury Basin, New Zealand

E.M. Crouch[1], C.L. Shepherd[1], H.E.G. Morgans[1], B.D.A. Naafs[2], E. Dallanave[3], A. Phillips[1], C.J. Hollis[1], R.D. Pancost[2]

[1]GNS Science, P.O. Box 30368, Lower Hutt, New Zealand

[2]Organic Geochemistry Unit, School of Chemistry, School of Earth Sciences, and Cabot Institute for the Environment, University of Bristol, UK

[3]Research Group Marine Geophysics, Faculty of Geosciences, University of Bremen, GEO Gebäude, Klagenfurter Straße, 28359 Bremen, Germany

Abstract

The Cretaceous–Paleogene marine sedimentary succession exposed in the banks of the middle reaches of the Waipara River (referred to as mid-Waipara), north Canterbury, New Zealand, has been the subject of several high-profile studies of Paleogene paleoclimate over the past decade. It is one of relatively few sections globally where a multi-proxy approach is possible due to the good preservation of microfossils and organic biomarkers. The Eocene section is also well dated by magnetostratigraphy and biostratigraphy based on planktic foraminifera, calcareous nannofossils and dinoflagellate cysts (dinocysts). Here, we build on this previous work and undertake a comprehensive analysis of paleontological and geochemical indicators of climatic and environmental changes through the early–middle Eocene part of the section, with particular focus on the Early Eocene Climatic Optimum (EECO; 53.26–49.14 Ma). We correlate a 33.5 m-thick interval with the EECO, based on biostratigraphy, magnetostratigraphy, TEX_{86}-paleothermometry and bulk carbonate $\delta^{13}C$. Our new sea-surface temperature (SST) record based on TEX_{86} agrees with a previous lower resolution record based on TEX_{86} and planktic foraminiferal $\delta^{18}O$ and Mg/Ca ratios. The EECO interval in this section extends from the upper part of the New Zealand Waipawan Stage to the Mangaorapan/Heretaungan Stage boundary at 49.27 Ma. The EECO onset is not exposed, but the termination is well constrained by a fall in SST and shift to more positive $\delta^{13}C$ values. Six negative carbon isotope excursions (CIEs) are recognised within the EECO and are tentatively correlated with CIEs J/K, M, O, Q, T and C22nH4 in the global $\delta^{13}C$ compilation. The CIEs are associated with warmer SSTs, indicating that they represent hyperthermals. The BAYSPAR TEX_{86} calibration indicates SST increased by as much as 12°C from the early Eocene (~55 Ma) to the EECO, where SST peaked at 35°C. SST gradually declined from mid EECO (~51 Ma) into the middle Eocene. The marked warming in the early EECO is associated with the highest abundance of warm-water taxa in calcareous nannofossil and dinocyst assemblages, the highest proportion of planktic foraminifera, and a coeval long-term shift to abundant angiosperm vegetation, primarily driven by a rise in Casuarinaceae. There is good agreement between TEX_{86} and marine microfossil-based proxies for temperature, providing confidence that both approaches are useful guides to past water temperature. Warm-water marine taxa are most abundant in

the EECO but are not dominant. Comparison of the abundance of nannofossil warm-water taxa between mid-Waipara and a low-latitude site on Shatsky Rise suggests the latitudinal temperature gradient between mid- and low-latitudes in the EECO was greater than the TEX_{86} proxy implies. There is no clear evidence for enhanced sedimentation rates associated with the EECO, in contrast to evidence from the nearby Mead Stream section. Superabundant *Homotryblium*, a euryhaline dinocyst, in the early and middle EECO suggests elevated salinity and/or stratified surface waters, and there is no clear evidence of increased surface productivity associated with the EECO. Declining SST in the late EECO, ~50 Ma, corresponds with an increase in cool-water taxa and terrigenous material. This article highlights the importance of combining well-calibrated paleontological and geochemical records to better constrain and understand past warm climate states.

1. Introduction

A succession of short- and long-term global warming events during the early Eocene (56–48 Ma) provide important insights into climate variability under background conditions of elevated atmospheric CO_2, generally exceeding 800 ppmv (Zachos et al., 2008; Anagnostou et al., 2016; Hollis et al., 2019). Well-calibrated sedimentary records for this time period from different regions are essential to understand the geographic variability in climate and ecosystem response and to validate Earth system models (Huber and Cabellero, 2011; Lunt et al., 2017). Records from the South Pacific are of particular interest because the Pacific Ocean was the primary driver of ocean heat transport during the Paleogene (Huber and Nof, 2006). Both model and proxy studies indicate that the Pacific sector of the Southern Ocean was a major source of deep water through most of the Paleogene (Littler et al., 2014; Huck et al., 2017). For this reason, the Southwest Pacific has been the focus of several studies of early Paleogene climate dynamics over the past two decades (e.g., Crouch et al. 2003; Nicolo et al., 2007; Bijl et al., 2009, 2013a; Hollis et al., 2009, 2012, 2015; Slotnick et al., 2012, 2015; Pancost et al., 2013; Taylor et al., 2013; Dallanave et al., 2014, 2016; Inglis et al., 2015; Hines et al., 2017; Naafs et al., 2018).

The lower Paleogene succession at mid-Waipara River, Canterbury Basin, New Zealand (Fig. 1), has been a focus of many of these studies because the siliciclastic sediments contain a wide range of microfossils as well as immature organic matter suitable for biomarker studies. Studies have investigated both marine and terrestrial temperature records from latest Cretaceous to middle Eocene, focusing on glycerol dialkyl glycerol tetraethers (GDGTs; Hollis et al., 2009, 2012, 2014; Pancost et al., 2013; Taylor et al., 2013, 2018) as well as Mg/Ca ratios and oxygen isotopes (Hollis et al. 2009, 2012; Creech et al. 2010; Hines et al., 2017). These studies have provided multiproxy estimates of temperature, which have been compared with climate and general circulation models (Huber and Caballero, 2011; Hollis et al., 2012; Lunt et al., 2012). The Eocene section also has a well-calibrated age model that incorporates dinocyst, foraminiferal and nannofossil biostratigraphy and magnetostratigraphy (Dallanave et al. 2016; Shepherd and Kulhanek, 2016). Whilst paleontology has supported these studies, the focus has been on biostratigraphy rather than paleontological indicators of

76 climatic and environmental change in the Eocene greenhouse world. In this article, we utilise the well-
77 preserved calcareous and organic-walled microfossil assemblages in this continental margin section to
78 evaluate proxy- and model-based climate reconstructions and to infer the biological response to
79 changes in climate and carbon cycling.

80 Our multidisciplinary study includes analysis of foraminiferal, calcareous nannofossil,
81 dinoflagellate cyst (dinocyst) and spore/pollen assemblages, bulk carbonate $\delta^{13}C$ isotopes, $CaCO_3$
82 content, and biomarkers (GDGTs), and utilises samples collected as part of our magnetostratigraphic
83 study (Dallanave et al., 2016) of the lower and middle Eocene succession at mid-Waipara River. We
84 document the timing and variability of environmental and climatic changes in the marine and
85 terrestrial realm, and compare these changes with a new and more detailed record of sea surface
86 temperature (SST) and carbon cycle change than has been previously reported for this section.

87

88 **2. Identifying the Early Eocene Climatic Optimum (EECO)**

89 The warmest sustained temperatures of the Cenozoic occurred in the EECO (Zachos et al.,
90 2001, 2008; Westerhold and Röhl, 2009; Lauretano et al., 2016; Evans et al., 2018) and were
91 associated with atmospheric CO_2 levels of >800 ppmv (Beerling and Royer, 2011; Anagnostou et al.,
92 2016; Boudreau et al., 2019; Hollis et al., 2019). The EECO (Fig. 2) was initially defined by a
93 minimum in oxygen isotope ($\delta^{18}O$) values of benthic foraminifera that lasted 2–3 Myrs, from ~53–50
94 Ma (Zachos et al., 2001; Kirtland Turner, 2014). Recent studies indicate that the EECO onset can be
95 tied to one of several carbon isotope excursions (CIEs) from the middle early Eocene (Cramer et al.,
96 2003; Westerhold et al., 2012; Lauretano et al., 2015, 2018). A new astronomically-tuned, benthic
97 foraminiferal record at ODP Site 1209, North Pacific, recommends that the J event, dated at 53.26
98 Ma, be adopted as the base of the EECO (Westerhold et al., 2018). In the hemipelagic succession of
99 eastern Marlborough, New Zealand (Fig. 1), this CIE coincides with a transition from limestone to
100 marl-dominated sediments (Hollis et al., 2005 a, b), which is inferred to reflect hydrological changes
101 linked to the EECO (Slotnick et al, 2012, 2015; Dallanave et al., 2014). The top of the EECO is tied to

a CIE in uppermost Chron C22n (C22nH5), dated at 49.14 Ma, that is coincident with the onset of a long-term cooling trend in the benthic $\delta^{18}O$ record (Westerhold et al., 2018).

Thus, the EECO is currently considered to extend from 53.26 Ma to 49.14 Ma, Chron C24n.2rH1 (J event) to uppermost Chron C22n (CIE C22nH5), an interval of 4.12 Myrs that extends from the upper part of calcareous nannofossil zone NP11 to lower NP14 (Hollis et al., 2019). In terms of New Zealand stages (Raine et al., 2015), the EECO extends from the late Waipawan to close to the Mangaorapan/Heretaungan boundary (49.27 Ma) and includes the Waipawan/Mangaorapan boundary at 52 Ma (Fig 2).

3. Previous early to middle Eocene studies at mid-Waipara River

The lower–middle Eocene Ashley Mudstone succession outcrops along the river bed (Fig. 1), and three sample suites have been collected (Supp. Information Fig. 1). Two suites, from 2003 and 2007, are integrated into one composite section (Morgans et al., 2005) and have been the focus of several studies, including $\delta^{13}C$ isotopes, Mg/Ca ratios, GDGT analyses, and biostratigraphy (Hollis et al., 2009, 2012; Creech et al., 2010; Pancost et al., 2013; Taylor et al., 2013; Inglis et al., 2015). As part of a magnetostratigraphic study (Dallanave et al., 2016), a third suite was taken in 2012 (Fig. 3) from the same river bed section as the 2003 collection. Oriented samples for paleomagnetic analyses were taken over a ~45 m stratigraphic interval. Six magnetic polarity reversals were correlated to magnetic polarity Chrons C23n.2n to C21 n, with the aid of nannofossil and foraminiferal biostratigraphy. This correlation spans from ~51.5–47 Ma, based on the orbitally-tuned Eocene timescale of Westerhold et al. (2017), and provides a magnetostratigraphically calibrated age for the base of the NZ Heretaungan Stage, i.e., 49.27 Ma (C22n(0.6)).

Following the recommendation of van Hinsbergen et al. (2015), our paleogeographic reconstruction (Fig. 1) and Eocene locations of the sites mentioned in the text are based on a paleomagnetic reference frame (Matthews et al., 2016). This reference frame is more suitable than a mantle-based reference frame for paleoceanographic and paleoclimate studies because it is tied to the

Earth's spin axis and therefore more accurately represents true paleolatitude. As noted by van Hinsbergen et al. (2015), this change in reference frame moves Southwest Pacific Paleogene sites northward by ~10° and the mid-Waipara site shifts from the previously reported paleolatitude of 55°S (e.g. Hollis et al., 2009, 2012) to 46°S (Fig. 1).

4. Material and methods

4.1 Mid-Waipara River section and samples

The mid-Waipara River section (Fig. 1) is situated ~13 km west of the Waipara township, north Canterbury, and includes the area downstream from Doctors Gorge to top of the Amuri Limestone in what is referred to as the 'lower gorge' (NZ Map Series 260, reference M34/755 946–M34/789 944). The Ashley Mudstone comprises low-dipping calcareous mudstone outcropping in the river bed (Morgans et al., 2005). Strata are well-exposed in the central part, but exposure is more variable in the upper and lower parts, and highly dependent on river level and sediment load. Samples are examined from two suites, the 2007 and 2012 collections (Fig. 3; Supp. Information Fig. 1). The two collections are correlated by biostratigraphy and lithology, as the reference marker used in the 2007 collection was washed away and direct field correlation was not possible. The base of the 2012 (M34/f930) and top of the 2007 (M34/f889) collections are inferred to be separated by a stratigraphic gap of ~1 m. Eleven samples (M34/f899–f889) were collected in 2007 from ~15 m of stratigraphic section, although the middle part of the section (-13.2 to -6.6 m) could not be sampled as the river level was too high. In 2012, a detailed suite of 118 samples (M34/f930–f1047) were taken from ~66.5 m of section.

4.2 Microfossils

Biostratigraphic and paleoenvironmental studies were completed for foraminifera, calcareous nannofossils, dinocysts, and spores and pollen. All paleontological samples, residues and slides are

153 stored in the National Paleontological Collection at GNS Science, Lower Hutt, NZ. Biostratigraphic
154 data are in the Appendix (Supp. Information).

155

156 *4.2.1 Foraminifera*

157 A total of 92 samples were processed, with 500 g of dried sediment washed over a 75 μm
158 screen for each sample. The residues were then dried, reweighed and half was retained for a
159 quantitative census. The remaining half of the residues were qualitatively picked to obtain a
160 comprehensive faunal assemblage that was used for biostratigraphy and paleodepth. A subsequent
161 count was completed to calculate the planktic/benthic foraminiferal ratio, and this value is expressed
162 as the proportion of planktic specimens in the total foraminiferal assemblage (planktic abundance).

163

164 *4.2.2 Calcareous nannofossils*

165 Smear slides were made for 34 samples using standard techniques (Bown and Young, 1998).
166 In some cases, samples contained a large amount of fine sand and strewn slides were prepared
167 according to the method of Bown and Young (1998). Slides were analysed using an Olympus BX53
168 microscope at 1000x magnification in plane-transmitted light (PL), cross-polarized light (XPL) and
169 phase contrast (PC) light. Relative abundance of taxa was determined from counts of 450 specimens
170 along random traverses of each slide, followed by scanning to identify additional rare species.
171 Specimens were identified to species level following the taxonomic concepts of Perch-Nielsen (1985),
172 Bown (1998, 2005), Dunkley Jones et al. (2009) and Shamrock and Watkins (2012). Results are
173 correlated to the zonation scheme of Martini (1971), with subzones as defined by Aubry (1991) and
174 absolute ages for events calibrated to Gradstein et al. (2012) and Hollis et al. (2019). Full synonymies
175 for all taxa mentioned in this paper are available in the publications listed above. To examine
176 paleotemperature changes, we distinguish cool- and warm-water taxa based on previous studies that
177 use statistical analyses of assemblage data (e.g., cluster analysis, principal component analysis) to
178 interpret patterns and relationships among taxa (e.g. Wei and Wise, 1990; Siesser, 1993; Bralower,

2002; Villa and Persico, 2006; Villa et al., 2008; Schneider et al., 2011; Shamrock and Watkins, 2012). Cool-water taxa comprise *Chiasmolithus* spp. and *Reticulofenestra daviesii*, while warm-water taxa comprise *Discoaster* spp., *Sphenolithus* spp. and *Coccolithus formosus*.

4.2.3. Palynomorphs

A total of 45 samples were processed using standard palynological processing techniques. Between 21 and 31 g of sediment was crushed, dried and the carbonate and siliceous component removed by adding 10% HCl and 50% HF, respectively. Samples were oxidised, for up to 10 minutes, using 70% HNO_3 and washed with 5% NH_4OH to disaggregate amorphous and organic debris. Some samples were placed in an ultrasonic bath (for up to 1 minute) prior to sieving. All samples were sieved over a 6 µm mesh, and well-mixed representative fractions of the >6 µm residue mounted on glass slides using a glycerine jelly medium. The relative abundance of palynomorphs was determined in three ways; 1) ~200 dinocysts counted for 43 samples, 2) ~ 200 spores/pollen counted for 33 samples, and 3) ~150 marine and terrestrial palynomorphs counted for 37 samples. At least one extra slide was scanned for additional rare species. Quantitative results are shown as a percentage of the total count, or with reference to the following: rare (1–5%), common (6–10%), frequent (11–20%), abundant (21–40%) and super abundant (>40%). Dinocyst biostratigraphy is correlated to the established New Zealand zonation (Morgans et al., 2004), with early Eocene zones based on Crouch (2001; Fig. 2). An alternative South Pacific zonation (Bijl et al., 2013a) is not utilised because several index species are either not present at mid-Waipara (e.g., lowest occurrence (LO) of *Arachnodinium antarcticum*) or seem to have diachronous ranges (e.g. highest occurrence (HO) of *Palaeocystodinium golzowense* is older in New Zealand than recorded at ODP Site 1172, East Tasman Plateau).

To examine paleotemperature changes, we distinguish taxa with a low-latitude (warm-water) affinity from those with a Southern Ocean (cooler-water) affinity. Our warm-water group includes taxa of the Wetzelielloideae subfamily: *Apectodinium*, *Charelsdowniea*, *Dracodinium*, *Rhombodinium*, *Wetzeliella* and *Wilsonidium*. The genus *Apectodinium* evolved in equatorial regions, with a LO close to the Danian/Selandian boundary (~61 Ma, Guasti et al., 2005; Awad and Oboh-

206 Ikuenobe, 2016), while other Wetzelielloideae taxa (*Rhombodinium*, *Wilsonidium*) have LOs in north-
207 east India (Prasad et al., 2006) and the Tethys (Iakovleva and Heilmann-Clausen, 2007) in sediments
208 dated as latest Paleocene. Recent work suggests the lower SST tolerance of Wetzelielloideae was 20 ±
209 2.5°C (Frieling et al., 2014). The genus *Homotryblium* also evolved in low latitudes, with a LO near
210 the base of the Thanetian (upper Foraminifera Zone P4a, Iakovleva et al., 2001; Crouch et al., 2003;
211 Slimani et al., 2016). We keep the *Homotryblium* genus separate from the Wetzelielloideae group as it
212 has a different morphology and may have had a broader SST range, from tropical–warm temperate
213 (Köthe, 1990; Brinkhuis, 1994), although a recent study suggests it is part of an epicystal
214 Goniodomideae ecogroup that preferred SSTs >25 ± 2.5°C (Frieling and Sluijs, 2018). Taxa
215 associated with the Endemic Antarctic Community (EAC), or transantarctic community (Wrenn and
216 Beckman, 1982; Bijl et al., 2011), are found south of ~45°S (Bijl et al., 2013b) and may have
217 preferred cooler Antarctica-derived surface currents, particularly in the late early Eocene–late Eocene
218 (Bijl et al., 2011, 2013b). In this study we identify a limited number of EAC taxa, comprising
219 *Alterbidinium assymetricum*, *Deflandrea antarctica*, *Enneadocysta* group and *Spinidinium*
220 *macmurdoense*. Whilst Bijl et al. (2013b) considered *Membranophoridium perforatum* to be part of
221 the EAC, we do not include this taxon as it appears to have extended north of 45°S in some regions
222 (Wilson, 1988).

223

224 *4.3 Stable isotopes and carbonate content*

225 A total of 68 samples were analysed for carbonate content and bulk carbonate $\delta^{13}C$ and $\delta^{18}O$
226 at the National Isotope Centre, GNS Science. Samples were analysed on the GVI IsoPrime
227 Preparation System at a reaction temperature of 25°C for 24 hours and run via dual inlet on the
228 IsoPrime mass spectrometer. All results are reported with respect to VPDB, normalised to an internal
229 GNS Marble standard (2.04‰ for $\delta^{13}C$ and -6.40‰ for $\delta^{18}O$). Precision is 0.1‰ for $\delta^{13}C$ and 0.2‰
230 for $\delta^{18}O$ (Appendix, Supp. Information).

231

232 *4.4 Organic geochemistry*

233 A total of 68 samples were analysed for glycerol dialkyl glycerol tetraethers (GDGTs) at the
234 Organic Geochemistry Unit, University of Bristol (Appendix, Supp. Information). Sediments were
235 freeze-dried and powdered with a pestle and mortar. Biomarker lipids were extracted from between 30
236 and 50 g of sediment using Soxhlet technique and 220 ml of a 9:1 mixture (v/v) of dichloromethane
237 (DCM) and methanol (MeOH). Sediments were extracted for 24 hrs at ~70 °C with activated copper
238 to remove elemental sulfur. The total lipid extract (TLE) was concentrated using a rotary evaporator,
239 then dried under a gentle flow of nitrogen. Open column flash chromatography (alumina) was used to
240 separate the TLE into apolar and polar fractions using 4 ml of dichloromethane (DCM):hexane (9:1)
241 and 4 ml of DCM:Methanol (MeOH) (1:2), respectively. Both fractions were fully dried under a
242 gentle flow of nitrogen. The polar fraction was redissolved in a mixture of hexane and *iso*-propanol
243 (IPA) (99:1) and filtered through a 0.45 µm PTFE filter. Filtered polar fractions were analysed for
244 their core-lipid GDGTs distribution by high performance liquid chromatography/atmospheric pressure
245 chemical ionisation-mass spectrometry (HPLC/APCI-MS) using a ThermoFisher Scientific Accela
246 Quantum Access triplequadrupole MS. Normal phase separation was achieved using two ultra-high
247 performance liquid chromatography silica columns, following the methods of Hopmans et al. (2016).
248 Injection volume was 15 out of 100 µl. Analyses were performed using selective ion monitoring mode
249 (SIM) to increase sensitivity and reproducibility (*m/z* 1302, 1300, 1298, 1296, 1294, 1292, 1050,
250 1048, 1046, 1036, 1034, 1032, 1022, 1020, 1018, 744, and 653). Sample results were integrated
251 manually using the Xcalibur software.

252

253 *4.5 GDGT-based calibrations and indices*

254 We used the distribution of isoprenoidal GDGTs as reflected in the TetraEther indeX of
255 tetraethers consisting of 86 carbon atoms (TEX_{86}) to reconstruct SST (Schouten et al., 2002).

256 $$\text{eq. (1) } TEX_{86} = \frac{[iso\text{GDGT-2}] + [iso\text{GDGT-3}] + [cre.regio\ isomer]}{[iso\text{GDGT-1}] + [iso\text{GDGT-2}] + [iso\text{GDGT-3}] + [cren.regio\ isomer]}$$

To capture the range of potential SST estimates that may be derived from this proxy we applied two different calibrations: the BAYSPAR deep time analogue calibration (Tierney and Tingley, 2014, 2015; Tierney et al., 2017), which is based on a linear relationship between TEX_{86} and SST, and the TEX_{86}^{H} calibration (Kim et al., 2010), which is based on an exponential relationship (Hollis et al., 2019). The TEX_{86}^{L} calibration is not used because it has been found to have significant shortcomings (Hollis et al., 2019). The BAYSPAR deep-time calibration has been applied to reconstruct SSTs during greenhouse periods such as the early Paleogene (Naafs et al., 2018), PETM (Tierney and Tingley, 2014) and Cretaceous (Naafs and Pancost, 2016; O'Brien et al., 2017). For the BAYSPAR calibration, we used a prior of 30 ± 20°C and search tolerance of 0.13. The resulting analogue locations are all located in the tropics or subtropics, including the Red Sea (this data is excluded from the TEX_{86}^{H} calibration). Selecting different values for the prior (e.g. 25–35°C) does not result in significantly different SST results. Although part of our data lies above the modern calibration range for TEX_{86}, the data lie within the range of mesocosm experiments that indicate TEX_{86} remains (linearly) correlated to temperature at SSTs up to 40 °C (Schouten et al., 2007). The BAYSPAR deep-time calibration incorporates this range into its error calculation.

Following Inglis et al. (2015) we identify an *iso*GDGT distribution similar to that found at present in the Red Sea (Trommer et al., 2009) using;

$$\text{eq. (2) isoGDGT}_{\text{rs}}(\%) = \frac{[cren.regio\ isomer]}{[cren.regio\ isomer] + [iso\text{GDGT-0}]} \times 100$$

In addition, we also calculate the Branched versus Isoprenoidal Tetraether (BIT) index (Hopmans et al., 2004).

$$\text{eq. (3) BIT} = \frac{Ia + IIa + IIa' + IIIa + IIIa'}{Ia + IIa + IIa' + IIIa + IIIa' + cren.}$$

BIT reflects the relative abundance of *br*GDGTs that are abundant in mineral soil and peat (Weijers et al., 2006; Weijers et al., 2007; Naafs et al., 2017b) versus a specific archaeal *iso*GDGT, crenarchaeol, produced by *Thaumarchaeota* that is more abundant in the marine realm (Sinninghe Damsté et al., 2002). High BIT values are typically found in soils and lacustrine archives, and are therefore

generally used to indicate a high input of terrestrial-derived GDGTs, which can result in unreliable SST estimates (Hopmans et al., 2004). However, it is important to note that brGDGTs can also be produced *in situ* in marine sediments and do not always purely reflect changes in terrestrial input (Sinninghe Damsté, 2016). BIT values <0.3 indicate terrestrial-derived GDGTs likely have little effect on TEX_{86}-based SST estimates (Hopmans et al., 2004).

The methane index (MI) (Zhang et al., 2011) is defined as;

$$\text{eq. (4) MI} = \frac{[iso\text{GDGT-1}] + [iso\text{GDGT-2}] + [iso\text{GDGT-3}]}{[iso\text{GDGT-1}] + [iso\text{GDGT-2}] + [iso\text{GDGT-3}] + [Cren.] + [cren.regio\ isomer]}$$

A MI >0.5 indicates a contribution of methanogens to the GDGT pool that can bias TEX_{86}-based SST.

5. Results

5.1 Stratigraphy, age control and fossil assemblages

The stratigraphy of the section is described in relation to five Eocene New Zealand Stages (Fig. 2): Waipawan, Mangaorapan, Heretaungan, Porangan and Bortonian (Cooper et al., 2004; Raine et al., 2015), which extend from earliest Eocene to latest middle Eocene (56 to 39.1 Ma). Biostratigraphic data are in the Appendix (Supp. Information).

5.1.1. Lithostratigraphy

The ~80 m section is mainly a moderately indurated, partly calcareous, grey mudstone, which is glauconite rich in the upper part of the section. An abrupt coarsening of sediment occurs at ~59 m, with overlying sediments containing common medium- to coarse-grained glauconite (Fig. 3). Magnetostratigraphy and calcareous microfossil biostratigraphy provide a good age framework (Dallanave et al., 2016). The section extends from lower–middle Eocene (~55.5–42 Ma; Waipawan–lower Bortonian), with an unexposed interval in the Waipawan part of the section (-13.1 to -6.7 m). The abrupt change in sediment type at 59 m coincides with an unconformity that spans ~3 Myr:

306 uppermost Heretaungan, Porangan and lowermost Bortonian (middle Eocene) sediments are not
307 preserved.

308

309 *5.1.2 Foraminifera*

310 Foraminifera are poorly preserved in the lowermost part of the section (-16.15 to -13.2 m),
311 but an earliest Eocene (Waipawan) age is inferred from identifiable specimens of *Globanomalina*
312 *australiformis* and *Morozovella aequa* (Fig. 3). Foraminifera are relatively well preserved, abundant
313 and diverse above the unexposed section, from -6.61 to 66.5 m, although preservation is poor above
314 59 m, coincident with the occurrence of greensand beds. The Waipawan/Mangaorapan boundary is
315 identified at -3.99 m based on the lowest occurrence (LO) of *Morozovella crater*. The base of the
316 Heretaungan stage is identified by the LO of the marker benthic species *Elphidium hampdenense* at
317 27.51 m, and the species is present up to 58.55 m. Two species of the genus *Morozovella*, *M. crater*
318 and *M. lensiformis*, are present in all samples from -3.99 to 57.9 m and the genus is only absent in the
319 uppermost Heretaungan sample (58.55 m). The primary datum for the Porangan Stage, benthic
320 species *Elphidium saginatum*, is not identified in the section. The base of the Bortonian is identified
321 by the primary datum, LO of *Globigerinatheka index*, directly above the unconformity at 59.71 m,
322 and is supported by the LOs *of Bulimina bortonica* at 59.71 m and *Acarinina primitiva* at 63.05 m.

323 Planktic foraminiferal abundance is low in the early Waipawan (average 3%) but increases to
324 >40% in the late Waipawan. Several pulses of high abundance, >70%, are seen in the early–middle
325 Mangaorapan, whereas the late Mangaorapan has stable planktic abundance (Fig. 3). There is a
326 general abundance drop in the Heretaungan, with the average value (38%) noticeably lower than in
327 the Mangaorapan (65%).

328

329 *5.1.3 Calcareous nannofossils*

330 A summary of the detailed calcareous nannofossil biostratigraphy by Shepherd and Kulhanek
331 (2016) is provided here. The presence of *Rhomboaster bramlettei* at -15.25 m places the base of the

section in Zone NP10, early Eocene (Fig. 3). The LO of *Sphenolithus radians* at -6.61 m is used as a secondary marker for the base of NP11 (Backman, 1986) rather than the index species *Tribrachiatus contortus*, which is absent. The LO of *Tribrachiatus orthostylu*s, an event within the upper part of NP10 (Pälike et al., 2010), co-occurs with the LO of *S. radians*, suggesting the upper part of NP10 is within the non-exposed interval from -13.2 to -6.6 m. The LO of *Discoaster lodoensis* at -2.87 m, earliest Mangaorapan, marks the base of NP12. It is possible that *D. lodoensis* has a delayed LO at mid-Waipara, given that in the nearby Mead Stream section the LO of *D. lodoensis* occurs ~36 m below the LO of *Morozovella crater* and at mid-Waipara these two bioevents occur within ~1 m (Supp. Information Fig. 2). The HO of *T. orthostylus*, marker for the base of NP13, is observed at 11.13 m and lower Chron C22r (mid-Mangaorapan). The absence of *Discoaster sublodoensis*, marker for the base of NP14, means the NP13/NP14 boundary cannot be identified. However, the base of NP14 is known to occur in lower Chron C22n (Hollis et al., 2019), which is well-defined at mid-Waipara. From this we infer that the NP13/14 boundary lies in the late Mangaorapan, between ~20.7 and 27 m. Some or all of Zone NP15 (i.e., late Heretaungan–latest Porangan) is inferred to be missing because the markers for the base of NP15 and base of Subzone NP15b (LOs of *Nannotetrina fulgens* and *Chiasmolithus gigas*, respectively) are not observed. The base of NP16 is difficult to identify as both the primary and secondary markers, *Blackites gladius* and *Nannotetrina alata/fulgens*, are not observed. However, *Reticulofenestra umbilicus* (>14μm) and *Reticulofenestra reticulata* both have LOs in Zone NP16 (Pälike et al., 2010) and at mid-Waipara they co-occur at 62.26 m, early Bortonian. This suggests the lower part of Zone NP16 is missing, given that *R. reticulata* evolved at least several hundred thousand years after *R. umbilicus* (Gradstein et al., 2012; Agnini et al., 2014). Nannofossil and foraminiferal biostratigraphy agree that the unconformity at ~59 m encompasses the latest Heretaungan–earliest Bortonian (Fig. 3).

Nannofossil preservation is linked to carbonate content in this section. A positive correlation is observed between carbonate content and the visual observation of preservation (VOP), as well as the relative abundance of *Zygrhablithus bijugatus*, a species sensitive to dissolution (Jiang and Wise, 2009; Fig. 4). Poorly preserved assemblages occur in the Waipawan (NP10) and upper Heretaungan

359 (NP14) parts of the section where $CaCO_3$ is <10% and generally <15%, respectively. The best-
360 preserved assemblages are in the Mangaorapan, from the base of Zone NP12 to NP13–lower NP14,
361 where $CaCO_3$ is >15%. An increase in taxon richness and diversity is seen from the base of NP12,
362 consistent with the increase in preservation. Overall, the covariance between preservation and
363 diversity indices suggests preservation is an important factor influencing diversity in this section
364 (Shepherd, 2017).

365

366 *5.1.4 Dinoflagellate cysts*

367 Dinocyst assemblages are generally abundant and well preserved. Integration of index taxa
368 (Wilson, 1988; Morgans et al., 2004) with magnetostratigraphy and calcareous microfossil
369 biostratigraphy allows the age control of key species to be improved (Fig. 3). In the Waipawan, the
370 LOs of several zonal taxa are recorded: *Samlandia delicata* (NZE2a, -15.25 m) and *Impagidinium*
371 *cassiculum* (NZE2b, -13.20 m) occur in nannofossil Zone NP10, whereas the LO of *Dracodinium*
372 *waipawaense* (NZE3) is in Zone NP11 (-6.61 m). The range of *Wilsonidium ornatum* (NZE4) is
373 restricted to the Mangaorapan (Zone NP12 to NP13; -2.87–17.83 m). The LOs of key taxa
374 *Charlesdowniea coleothrypta* (19.98 m) and *Charlesdowniea edwardsii* (22.14 m) occur in the late
375 Mangaorapan. The HO of *C. coleothrypta* (26.75 m) is in upper Chron C22n, close to the
376 Mangaorapan/Heretaungan boundary, and the HO of *C. edwardsii* is early Heretaungan (32.40 m).
377 The onset of common–frequent *Membranophoridium perforatum*, a regional bioevent (Wilson, 1984,
378 1988), occurs in the Heretaungan close to the Chron C21r/C21n boundary.

379 Additional taxa offer potential to further refine the early–middle Eocene zonation. The LO of
380 *Impagidinium crassimuratum* and HO of *Manumiella rotunda* occur in Zone NP10 (early Waipawan).
381 The LOs of *Membranophoridium perforatum*, *Schematophora obscura* and the genus *Homotryblium*
382 are in Zone NP11 (late Waipawan). The LO of *Danea crassimuratum* is in Zone NP12 (early
383 Mangaorapan). The LO of *Achilleodinium biformoides*, *Deflandrea antarctica* and *Impagidinium*
384 *parvireticulum* are in Chron C22n (late Mangaorapan). The HO of the *Apectodinium* genus is close to
385 the Chron C22r/C22n boundary, late Mangaorapan. Fewer bioevents are seen in the Heretaungan.

386 Endemic Antarctic Community taxa (Bijl et al., 2011), *Alterbidinium assymetricum* and *Spinidinium*
387 *macmurdoense*, have LOs in lower Chron C21r, correlated with Zone NP14.

388

389 *5.1.5 Spores and pollen*

390 Spore and pollen abundance ranges from 22–43% of the total palynomorph assemblage.
391 Three zones (Raine, 1984; Morgans et al., 2004) are identified: PM3b, MH1 and MH2 (Fig. 3). The
392 lower part of the section (-16.15 m to -13.2 m) is correlated with the earliest Eocene PM3b Zone,
393 based on thermophilic taxa *Cupanieidites orthoteichus* and *Spinizonocolpites prominatus*, and rare
394 *Myricipites harrisii* (Raine et al., 2009; Handley et al., 2011). The base of Zone MH1, defined by a
395 noticeable increase in *M. harrisii* abundance, occurs between -13.2 m and -6.61 m (late Waipawan).
396 *M. harrisii* is common–abundant from this level to the late Heretaungan (57.93 m) and this interval is
397 correlated with Zone MH1. The tropical-subtropical spore *Crassoretitriletes vanraadshooveni*
398 (*Lygodium*) has a HO in the late Mangaorapan. The overlying Bortonian interval is correlated with
399 Zone MH2 based on the presence of *Nothofagidites flemingii*.

400

401 *5.2 Carbonate content, and carbon and oxygen isotopes*

402 Carbonate ($CaCO_3$) content is relatively low in the mid-Waipara section, never >30% (Fig.
403 5a). It is <15% in the earliest Eocene (early Waipawan) and most of the middle Eocene
404 (Heretaungan–early Bortonian). The highest $CaCO_3$ values, albeit variable, are in the late Waipawan
405 and Mangaorapan (early Eocene), also where well-preserved and abundant calcareous microfossil
406 assemblages are recovered. The primary source for $CaCO_3$ in this section is assumed to be calcareous
407 nannofossils. Variation in the relative abundance of planktic foraminifera suggests that the secondary
408 source may vary from calcareous benthic foraminifera in the early Waipawan and Heretaungan–
409 Bortonian, to planktics in the Mangaorapan. $CaCO_3$ content has a weak negative correlation with bulk
410 carbonate $\delta^{13}C$ ($r = -0.25$, $n = 68$, $p < 0.05$), is not correlated with $\delta^{18}O$, and has a strong positive
411 correlation with TEX_{86} ($r = 0.60$, $n = 68$, $p < 0.001$). Under typical ocean conditions, benthic

412 foraminifera will have lower $\delta^{13}C$ values than planktic foraminifera because the biological carbon
413 pump delivers ^{12}C-enriched organic matter to the sea floor.

414 Bulk carbonate $\delta^{13}C$ values range from -0.8‰ to 1.6‰, with a general trend towards higher
415 values from early to middle Eocene (Fig. 5b). A positive excursion, of ~1‰, occurs in the earliest
416 Eocene (early Waipawan). The most negative $\delta^{13}C$ value in the section, -0.8‰, is recorded at -6.61 m
417 in the late Waipawan, Zone NP11, and marks the first of a series of six (#1–6) negative carbon isotope
418 excursions (CIEs) in the Waipawan–Mangaorapan (early Eocene), which are superimposed on a
419 positive $\delta^{13}C$ trend. The $\delta^{13}C$ minimum within each CIE also increases over time, from -0.7‰ at -2.12
420 m to 0.7‰ at 26.75 m. A baseline positive shift (0.7–1.5‰) is recorded across the
421 Mangaorapan/Heretaungan boundary. Through most of the Heretaungan $\delta^{13}C$ values remain stable,
422 although a shift to lower values occurs in the late Heretaungan between ~50 and 59 m. The Bortonian
423 section is marked by variable $\delta^{13}C$ values, from -0.2‰ to 1.4‰, with a possible negative CIE at 62.26
424 m. The CIEs tend to be associated with lower $CaCO_3$ values but not in all cases (e.g., CIEs #3 and
425 #5). Some of the negative shifts in $\delta^{13}C$ in the earliest Waipawan and Heretaungan may be partly due
426 the low abundance of planktic foraminifera, because benthic foraminiferal calcite is generally more
427 enriched in ^{12}C. However, the lack of a consistent relationship between the CIEs in the late Waipawan
428 and Mangaorapan and planktic abundance suggests that foraminiferal calcite is not the primary source
429 of carbonate in this interval.

430 The bulk carbonate $\delta^{18}O$ record is not correlated with other geochemical proxies (Appendix,
431 Supp. Information Fig. 3) and the general trend is inconsistent with other early Eocene $\delta^{18}O$ records
432 (e.g., Westerhold et al., 2018; Barnet et al., 2019). Values in the range of -2.5 to -4‰ yield
433 temperatures in the range of 22–30°C, which are consistent with SSTs reported in previous studies
434 (Hollis et al., 2009, 2012). However, these values are interspersed with $\delta^{18}O$ values that range from -4
435 to -6.4‰ and yield unrealistically hot temperatures (up to 42°C). These values are likely to result
436 from post-depositional interactions with ^{18}O-depleted meteoric water (Hollis et al., 2012). Because we
437 have no way of discriminating between reliable and unreliable values, the bulk oxygen $\delta^{18}O$ record is

not discussed further in this article. The bulk carbonate $\delta^{13}C$ record is not affected by meteoric water interactions.

5.3 GDGT distributions

Both isoprenoidal and branched GDGTs are present in all samples, and the TEX_{86} and BIT records are broadly consistent with previously reported Eocene records from this section (Hollis et al., 2009, 2012). The most notable change in the TEX_{86} record is in the basal part of the section, where values increase from 0.65–0.7 in the early Waipawan to >0.8 in the late Waipawan (Fig. 5c). These high TEX_{86} values continue up to 5.23 m in the early Mangaorapan (Chron C23n.2n). The overlying TEX_{86} record is characterized by a gradual decline into the middle Eocene, with a sharp decrease at the Mangaorapan/Heretaungan boundary. Average TEX_{86} values in the Heretaungan are lower (0.7) than in the Mangaorapan (0.8). TEX_{86} values in the early Bortonian, Zone NP 16, are variable and range between 0.55 and 0.7. There is a strong negative correlation ($r = -0.54$, $n = 68$, $p < 0.001$) between TEX_{86} and bulk carbonate $\delta^{13}C$. Most early Eocene CIEs appear to be associated with higher TEX_{86}, implying that these CIEs represent hyperthermals.

The methane index (MI) is ≤ 0.30 in all samples, indicating that TEX_{86} values are not biased by a large contribution of methanogens to the GDGT pool. Low BIT indices (<0.25) throughout the section indicate that TEX_{86} values are likely not significantly biased by terrestrial input. BIT values are lowest (<0.1) in the Waipawan and increase progressively through the overlying Mangaorapan and Heretaungan Stages (Fig. 5d). The BIT index is highly variable in the early–middle Mangaorapan (Zone NP12), with lower values associated with the hyperthermals (high TEX_{86}) and higher values associated with positive excursions in bulk carbonate $\delta^{13}C$. Overall, the BIT index exhibits a weak negative correlation with TEX_{86} and a strong positive correlation with $\delta^{13}C$ ($r = -0.24$, $p < 0.05$ and 0.65, $p < 0.001$, respectively, $n = 68$). The anticorrelation between the BIT index and $\delta^{13}C$ is difficult to interpret, if we assume the BIT index purely reflects changes in terrestrial input, particularly the decrease in BIT and, hence, terrigenous supply during the negative CIEs. Previous studies in Eocene sections to the north (Marlborough, Fig. 1) have shown that hyperthermals are associated with

465 increased terrigenous input in bathyal settings (Hollis et al., 2005a; Nicolo et al., 2007; Slotnick et al.,
466 2012, 2015), and this would be expected to be associated with an increase in BIT values. At mid-
467 Waipara, however, we observe a decrease in BIT values during negative CIEs, which implies reduced
468 terrigenous input and may be a localised response to transient climate events, such as current
469 winnowing of finer sediments. However, the BIT index can be influenced by other factors and does
470 not always purely represent a simple two end-member model between pure marine and terrestrial
471 input. For example, the reduced BIT could reflect a relative increase in crenarchaeol over brGDGT
472 input during the hyperthermals, or the BIT may respond to changes in the contribution of *in situ*
473 produced brGDGTs to the sedimentary GDGT pool. Either way, the low BIT values indicate that a
474 relatively low amount of the GDGT pool is derived from soils.

475 The brGDGTs found in these marine samples (Appendix) could also contain brGDGTs
476 generated in the water column or marine sediments, rather than from land-based soils, which
477 complicates the use of brGDGTs in these sediments to quantify terrestrial temperature (De Jonge et
478 al., 2014b; Sinninghe Damsté, 2016). A non-soil source of brGDGTs to the sediments at mid-Waipara
479 is further supported by the observation that the relative abundance (%) of penta- or hexamethylated
480 versus tetramethylated brGDGTs is higher than that seen in any modern mineral soil or peat (Supp.
481 Information Fig. 4). The number of rings of pentamethylated brGDGTs versus the number of rings of
482 hexamethylated brGDGTs is also significantly higher than that seen in any modern mineral soil or
483 peat. We therefore do not discuss brGDGT-based terrestrial temperatures at mid-Waipara River.

484

485 *5.4 The Early Eocene Climatic Optimum in the mid-Waipara River section*

486 A combination of biostratigraphy, magnetostratigraphy, bulk carbonate $\delta^{13}C$ values and
487 TEX_{86} is used to determine the position of the EECO in the mid-Waipara section. As discussed
488 earlier, the EECO is inferred to extend from 53.26–49.14 Ma, Chron C24n.2r (J event, mid-NP11) to
489 uppermost Chron C22n (C22nH5 event, lower NP14) (Westerhold et al., 2018). The lowest chron
490 identified in mid-Waipara is C23.2n, which lies in Zone NP12 (Fig. 5). The interval directly overlying
491 the unexposed interval in the lower part of the section (Waipawan, -6.61 m) is correlated with NP11,

492 has the highest TEX_{86} values in the section, and also has what we infer to be the first of six CIEs in
493 the section. For these reasons, we place the base of the EECO at this level (Fig. 6). There are
494 uncertainties, however, constraining the age of the lower part of the section (Supp. Information Fig.
495 2), and we infer the CIE at this level (#1) to correspond with either the J event (C24n.2rH1) or the K
496 event (C24n.1nH1). The upper limit of the EECO in this section is well recorded. We place it at the
497 uppermost CIE (#6), which lies within upper Chron C22n and coincides with the onset of a cooling
498 trend in the TEX_{86} record (Fig. 5). Given the age of the Mangaorapan/Heretaungan boundary, at 49.27
499 Ma (C22n(0.6)) and magnetostratigraphy in this part of the section, we infer CIE #6 to correspond
500 with the C22nH4 event (49.25 Ma). This suggests that cooling at mid-Waipara began slightly earlier
501 than the top EECO as recognised by Westerhold et al. (2018) at 49.14 Ma (C22nH5).

502 Combining these two datums with the integrated magnetobiochronology for the section
503 (Appendix, Supp. Information), calibrated to the timescale of Westerhold et al. (2017), allows us to
504 provisionally correlate the other CIEs in the section as follows: #2 = C23rH2 or M event; #3 =
505 C23n.2nH2 or O event; #4 = C22rH1 or Q event; #5 = C22rH4 or T event (Fig. 6). The major positive
506 shift in $\delta^{13}C$ during C23n (51.2–51 Ma; Westerhold et al., 2018) is not clearly observed at mid-
507 Waipara, perhaps due to the presence of cryptic unconformities in this part of the section.

508

509 *5.5 Paleoenvironmental changes*

510 *5.5.1 Foraminiferal assemblage*

511 Benthic foraminiferal paleodepth indicators (e.g. *Pleurostomella*, *Stilostomella* and
512 *Bathysiphon* spp.) suggest that the entire section was deposited in a middle bathyal setting (Appendix,
513 Supp. Information). The incoming of *Nuttallides carinotrumpyi* and the genera *Karreriella* and
514 *Vulvulina* in the early EECO (late Waipawan and early Mangaorapan) indicate a deeper bathyal
515 setting. The presence of *Tritaxilina zealandica*, from mid EECO to earliest post-EECO (middle
516 Mangaorapan–early Heretaungan), suggests that this is the deepest interval in the section, probably
517 lower bathyal (Hayward, 1986; Hayward et al., 2010). Foraminiferal assemblages higher in the post-

EECO Heretaungan indicate shallowing with the disappearance of *Karreriella* and *T. zealandica*, although middle bathyal indicators persist into the Bortonian.

Foraminiferal assemblages are affected by preservation. The best-preserved assemblages are in the late Waipawan–Mangaorapan (EECO) where $CaCO_3$ content is highest. Planktic abundance (Fig. 3) is also correlated with carbonate content ($CaCO_3$, r = 0.76, n = 26, p <0.001) although this may be due to a combination of factors, such as improved preservation and warmer conditions. Peaks in planktic abundance align with three of the negative CIEs (#1, 2, 5) and may be directly related to warmer SST or indirectly linked to warming by increased clay content, which can enhance preservation (Hollis et al., 2019). However, we have not confirmed that CIEs in this section are accompanied by an increase in clay. A strong correlation with TEX_{86} (r = 0.84, n = 26, p <0.001) provides further evidence that planktic abundance is linked to temperature. In the early Waipawan (below the EECO), a combination of cooler SST (Fig. 5c) and poor preservation perhaps led to low planktic abundance, despite the middle bathyal depositional setting. A similar trend is evident in the late Heretaungan.

5.5.2 Dinocyst assemblage

Gonyaulacoid dinocysts, representative of autotrophic dinoflagellates (Dale, 1996), dominate the Eocene assemblages and include the genera *Spiniferites*, *Operculodinium*, *Cerebrocysta* and *Impagidinium* (Fig. 7). Peridinioids (e.g., *Spinidinium* spp.), predominantly heterotrophic dinoflagellates, comprise <30% of the assemblage, apart from an interval in the late EECO (late Mangaorapan) where they become super-abundant. Assemblages below the EECO, early Waipawan, are dominated by cosmopolitan taxa, such as *Elytrocysta* spp., *Operculodinium* spp. and *Spiniferites* spp., and peridinioids are frequent. Compared with the early Waipawan, assemblages in the EECO (late Waipawan–Mangaorapan) are more diverse, with new taxa (e.g., *Batiacasphaera* spp., *Membranophoridium perforatum*, *Schematophora obscura*) becoming common, some cosmopolitan taxa (e.g., *Elytrocysta* spp., *Operculodinium* spp.) declining in abundance, and taxa such as *Diphyes* spp., *Hystrichokolpoma* spp. and *Impagidinium cassiculum* increasing in abundance. The tropical–

545 warm temperate genus *Homotryblium* is frequent–abundant in the early and middle EECO, with three
546 main abundance peaks ranging from 19–30%. In the late EECO, there is a significant increase (up to
547 40%) in peridinioid abundance, and they continue to be frequent–abundant in the overlying post-
548 EECO Heretaungan. Early Bortonian samples are a mix of cosmopolitan and more endemic (e.g.,
549 *Enneadocysta*) taxa.

550

551 *5.5.3 Spore and pollen assemblage*

552 Spores and pollen average 37% of palynomorph assemblages below the EECO (Fig. 8). This
553 abundance declines in the early–middle EECO, with a minimum value of 22% in Chron C22r, begins
554 to increase in the late EECO, and increases slightly in the post-EECO Heretaungan. Spore and pollen
555 abundance has a strong negative correlation ($r = -0.61$, $n = 35$, $p < 0.001$) with TEX_{86} and a moderate
556 positive correlation ($r = 0.33$, $n = 35$, $p < 0.05$) with BIT index. The parallel trend of increasing
557 terrestrial palynomorphs and BIT index in the late EECO and post-EECO Heretaungan suggests an
558 increasing contribution of terrestrial material in the sedimentary record as temperatures cooled
559 following the peak-EECO warmth.

560 Pre-EECO assemblages are dominated by gymnosperm pollen (up to 71%), particularly
561 *Podocarpidites* and the Araucarian taxon *Dilwynites granulatus*, and *Cyathidites* fern spores (Fig. 8).
562 In contrast, the early EECO shows a marked increase in angiosperm pollen, from <15% in the early
563 Waipawan up to 44% in the early Mangaorapan, and a concomitant decline in gymnosperm
564 abundance, most notably *Podocarpidites*. This angiosperm increase is mainly driven by a rise in
565 Casuarinaceae (*Myricipites harrisii*), although other angiosperms become more common, including
566 *Malvacipollis subtilis*, *Proteacidites* and *Tricolporopollenites latizonatus*. Vegetation remains
567 relatively stable in the EECO, with only a minor increase in *D. granulatus* and *Podocarpidites*
568 gymnosperms in the late EECO. The abundance of *M. harrisii*, and total angiosperms, decline slightly
569 in the Heretaungan and continue to decline in the early Bortonian, along with the incoming of the
570 cooler southern beech family Nothofagaceae genus *Nothofagus* (*Nothofagidites flemingii*).

571

572 *5.6 Microfossil paleotemperature indicators*

573 The relationship between microfossil assemblages and latitudinally constrained
574 environmental parameters, such as temperature and salinity, has been widely used to define
575 biogeographic zones, both in the modern ocean (e.g., McIntyre and Bé, 1967; Okada and Honjo,
576 1973; Prebble et al., 2013; Zonneveld et al., 2013) and in the geological record (e.g. Haq, 1981;
577 Hennissen et al., 2017). Whilst many environmental parameters have the potential to influence
578 microfossil distribution, SST has been shown to be the most important variable for calcareous
579 nannofossil (e.g., Haq et al., 1977; Haq, 1981; Wei and Wise, 1990) and dinocyst assemblages (e.g.,
580 De Vernal et al., 2005; Sluijs et al., 2005; Prebble et al., 2016; Frieling and Sluijs, 2018).

581 Warm-water indicators in the calcareous nannofossil assemblage, namely *Discoaster* spp.,
582 *Sphenolithus* spp. and *Coccolithus formosus*, are most abundant in the early and middle EECO, with a
583 combined abundance up to 19% (Fig. 4). The combined abundance of this warm-water group is also
584 high in the early Waipawan, below the EECO, and in the latest Heretaungan, post-EECO. This,
585 however, is due to the high preservation potential of *Discoaster* spp., which dominates the warm-
586 water assemblage in these intervals. In the EECO, cool-water indicators comprise <8% of the
587 assemblage, and they become more abundant (up to 17%) in the post-EECO Heretaungan. Initially,
588 the increase in cool-water taxa is related to an increase in *Reticulofenestra daviesii*, which is followed
589 by an increase in *Chiasmolithus* spp. in the late Heretaungan. The cool-water group has a moderate
590 negative correlation ($r = -0.43$, $n = 30$, $p < 0.02$) with TEX_{86}, whereas the warm-water group has a
591 weak positive correlation ($r = 0.30$, $n = 30$, $p < 0.1$); the weaker correlation is likely due to the
592 preservational effects noted above.

593 The abundance and diversity of the warm-water Wetzelielloideae dinocyst group is highest in
594 the EECO, comprising up to 7% of the assemblage and 7 taxa, and the group disappears entirely in the
595 post-EECO (Fig. 7). The warm temperate–tropical genus *Homotryblium* is first seen in the earliest
596 EECO and is abundant (up to 30%) in the early and middle EECO, and generally lower in the post-
597 EECO. The warm-water Wetzelielloideae group has a strong positive correlation ($r = 0.59$, $n = 41$, p

598 <0.001) with TEX_{86}, and there is a weak positive correlation (r = 0.29, n = 41, p <0.1) between
599 *Homotryblium* and TEX_{86}. Taxa of the Endemic Antarctic Community (EAC) group are first noted in
600 the late EECO, with abundance progressively increasing (up to 17%) in the post-EECO. The EAC
601 group has a strong negative correlation (r = -0.56, n =41, p <0.001) with TEX_{86}. These correlations
602 between calcareous nannoplankton and dinocyst fossil assemblage-based proxies for temperature and
603 the independent SST proxy, TEX_{86}, provide convincing evidence that both approaches are reliable
604 guides to past water temperature.

605 The main vegetation change is an increase in angiosperm pollen, driven by a rise in
606 Casuarinaceae (*Myricipites harrisii*) in the early EECO (Fig. 8). *M. harrisii* abundance has a strong
607 positive correlation with TEX_{86} (r = 0.76, n = 33, p <0.001). Angiosperms with affinities to
608 mesothermal–megathermal climates, such as *Anacolosidites*, *Bluffopollis scabratus*,
609 *Intratriporopollenites notabilis* and *Margocolporites cribellatus*, are rare but occur below, in, and
610 above the EECO (Appendix, Supp. Information). Most of these taxa do not occur in the cooler early
611 Bortonian, but the thermophilic *Spinizonocolpites prominatus* (*Nypa* mangrove) and *Malvacipollis*
612 *subtilis* taxa continue to be present.

613

614 *5.7 Sea-surface temperature*

615 While the evidence above, as well as numerous other multiproxy studies, show that TEX_{86} is
616 a robust guide to relative changes in SST (e.g., Zachos et al., 2005; Pearson et al. 2007), there is
617 ongoing debate about how the proxy relates to absolute temperature in the Paleogene, and especially
618 to mean annual SST in middle–high latitudes (Hollis et al., 2012). Here we use the two most widely
619 used calibrations, TEX_{86}^{H} (Kim et al., 2010) and $BAYSPAR_{SST}$ (Tierney and Tingley, 2015), which
620 yield similar absolute values in this record (Fig. 9a). TEX_{86}^{H} is based on an exponential relationship
621 with SST whereas BAYSPAR assumes a linear relationship, which results in higher values at the
622 upper end of the calibration (i.e. where TEX_{86} > 0.7) and especially beyond the range of the modern
623 calibration dataset. In our record, the amplitude of SST change is larger in $BAYSPAR_{SST}$ than in
624 TEX_{86}^{H} (Fig. 9b).

625 The most marked shift in SST is in the Waipawan, from pre-EECO to early EECO, with an
626 increase of between ~7 and 12°C (Fig. 9b). BAYSPAR SST increases from ~22.5 to 35.5°C, whereas
627 TEX_{86}^{H} SST increases from ~26 to 33.5°C. SST is highest in the early EECO and declines slightly
628 through the middle and late EECO. The baseline shift to a lower SST in Chron C23n.2n (~5.2 m),
629 corresponding with the C23n.2nH2 or O Event (Fig. 6), matches North Pacific records that indicate
630 the end of the warmest interval in the EECO occurs in uppermost Chron C23n.2n at 51.23 Ma
631 (Westerhold et al., 2018). A decrease in TEX_{86}-derived SST occurs across the
632 Mangaorapan/Heretaungan boundary, and SST continues to decline in the post-EECO Heretaungan.
633 Lower SST is present in the early Bortonian (middle Eocene, Zone NP16), although a transient peak,
634 up to 25.2°C ($BAYSPAR_{SST}$) and 27.9°C (TEX_{86}^{H}), is recorded and may represent the Middle Eocene
635 Climatic Optimum (MECO) at ~40 Ma.

636

637 *5.8 Red Sea-type GDGT distributions*

638 The $\%GDGT_{RS}$ distribution is used to identify sediments with unusually low amounts of
639 GDGT-0 relative to crenarchaeol regioisomer, which is characteristic for the GDGT distribution
640 found in modern sediments from the Red Sea (Trommer et al., 2009). Where $\%GDGT_{RS}$ >30 it is
641 inferred that the distribution is similar to that found in the Red Sea and may have added a warm bias
642 to SST estimates (Inglis et al., 2015). $\%GDGT_{RS}$ values >30 are common during times of elevated
643 warmth but may be a response to factors other than temperature given the distinct Red Sea archaeal
644 assemblages (Trommer et al., 2009). Crucially, the modern Red Sea data exert a particularly strong
645 influence on the high temperature end of all TEX_{86}-SST calibrations, depending on how they are
646 included (Inglis et al., 2015). At mid-Waipara River, $\%GDGT_{RS}$ values >30 are consistently observed
647 in the EECO, with the highest values in the early and middle EECO (Fig. 9c). $\%GDGT_{RS}$ values drop
648 to <30 across the Mangaorapan/Heretaungan boundary. $\%GDGT_{RS}$ values are <30 in the early
649 Waipawan (pre-EECO), Heretaungan (post-EECO) and early Bortonian.

650

6. Discussion

6.1 Comparison of proxy-based SST and microfossil records in the early and middle Eocene

Many early Paleogene studies have attempted to integrate climate proxy data with climate model simulations to understand global climate and carbon cycle response to elevated temperatures and greenhouse gases. While progress has been made in reconciling proxy temperature reconstructions with climate model simulations (Carlson and Caballero, 2017; Naafs et al., 2018), there remain known problems and inconsistencies with geochemical-based temperature proxies (Hollis et al., 2012, 2019). Multiproxy SST reconstructions (Mg/Ca ratios and $\delta^{18}O$ values of foraminiferal tests and GDGT-based TEX_{86} values) have been completed for the early–middle Eocene at mid-Waipara (Hollis et al., 2009, 2012; Inglis et al., 2015). The new TEX_{86}-based SST record presented here validates and complements these previous reconstructions (Fig. 10). The absolute SST values, however, remain debatable because they imply a reduced latitudinal temperature gradient between middle and low latitudes in the EECO and into the post-EECO, compared to the present (Cramwinckel et al., 2018; Naafs et al., 2018). In this context, the particularly warm temperatures (>30°C) in the Southwest Pacific warrant further investigation. Microfossil assemblages offer a means to explore these geochemical-based SST proxies and assess the faunal/floral evidence for tropical SSTs during the EECO in mid-latitudes (paleolatitude ~46°S) of the Southwest Pacific. We have found a good correlation between the trends in the TEX_{86} SST proxy and water temperature indicators within calcareous nannofossil and dinocyst assemblages.

Comparison of early–middle Eocene nannofossil assemblages from mid-Waipara with coeval records from subtropical (Shatsky Rise), temperate (Exmouth Plateau and Campbell Plateau) and subpolar (Kerguelen Plateau) provinces indicate that mid-Waipara assemblages are most similar to the other temperate sites, rather than assemblages at the subtropical setting (Fig. 11). Warm-water taxa (*Coccolithus formosus*, *Discoaster* spp., *Sphenolithus* spp.) are most abundant in the EECO at mid-Waipara, reaching up to 19% of the total assemblage. This is comparable with Site 762 (paleolatitude ~38°S), Exmouth Plateau, where warm-water taxa comprise up to 24% in the EECO (Schneider et al., 2011), and Site 277 (paleolatitude ~54°S), Campbell Plateau (Shepherd, 2017). Warm-water taxa at

678 the subtropical Site 1210 (paleolatitude ~28°N), Shatsky Rise, comprise up to 49% in the EECO
679 (Schneider et al., 2011). Indeed, there is a three-fold increase in the abundance of warm-water taxa in
680 the EECO between mid-Waipara (average 11%) and Site 1210 (average 35%). Conversely, cool-water
681 taxa (*Chiasmolithus* and *Reticulofenestra* spp.) are notably more abundant in the EECO, up to 18%, at
682 the polar Site 1135 (paleolatitude ~59°S), Kerguelen Plateau (Schneider et al., 2011), compared to
683 <10% at mid-Waipara, Campbell Plateau and Exmouth Plateau temperate sites. Cool-water taxa do
684 not significantly increase in abundance at mid-Waipara and Site 277 until after the EECO (Fig. 11).

685 Dinocyst assemblages at mid-Waipara exhibit a trend that is comparable to nannofossil
686 observations. The abundance and diversity of the warm-water Wetzelielloideae group is highest in the
687 EECO but the group comprises only a minor component (<10%) of the total assemblage (Fig. 12e). It
688 is estimated the lower SST tolerance of Wetzelielloideae was 20 ± 2.5°C (Frieling et al., 2014,
689 Frieling and Sluijs, 2018). Representatives of the Wetzelielloideae group are present below the EECO
690 and the group disappears above the EECO; however, TEX_{86}-based SST is well above 20°C in this
691 Waipawan–Heretaungan interval (Fig. 12b). This suggests that the disappearance of the group may be
692 linked to other factors in addition to cooling, such as changes in nutrients or fresh-water input. The
693 warm temperate–tropical genus *Homotryblium* peaks in abundance, up to 30%, in the lower–middle
694 EECO. The continued presence of *Homotryblium* above the EECO and in the early Bortonian
695 indicates a tolerance to a broader SST range than the Wetzelielloideae group, in contrast to
696 suggestions it preferred SSTs >25°C (Frieling and Sluijs, 2018), or perhaps an evolutionary
697 adaptation to post-EECO cooling (e.g., Dybkjær, 2004). The high *Homotryblium* abundance in the
698 EECO may be due to a combination of high SST and specific surface-water conditions (see section
699 6.3). The cooler-water EAC group first appear at mid-Waipara in the late EECO and, as with
700 nannofossils, become more common in the post-EECO (Fig. 12d, e). The increase in these cooler-
701 water groups suggests that the temperature gradient between the middle and low latitudes was
702 increasing in the post-EECO middle Eocene, perhaps related to tectonic processes such as the
703 deepening of the Tasmanian Gateway (Bijl et al., 2013b; Sijp et al., 2016).

Calcareous and organic marine microfossils from mid-Waipara show that elements of low-latitude provinces existed in the early Eocene in the New Zealand region and became more diverse and abundant in the EECO, but that marine assemblages characteristic of low-latitude Eocene oceans were by no means dominant in the extended period of early Eocene warmth. In fact, nannofossil assemblages indicate that temperature gradients between mid- and low-latitudes in the EECO were greater than indicated by geochemical SST proxies. In the EECO, there are three times as many warm-water indicators in the nannofossil assemblage at the low-latitude Shatsky Rise site (average 35%) as there are at the mid-latitude mid-Waipara section (average 11%). This is in contrast with geochemical-based SST proxies, where average SSTs in the EECO only differ by 5°C across the same latitudinal range and climate zones.

Despite these apparent discrepancies between absolute temperature inferred from geochemical proxies and fossil biogeography, microfossil assemblages and SST proxies are in good agreement in the trend of relative temperature change in the early–middle Eocene. TEX_{86}-based records indicate pronounced warming of between ~7 and 12°C (Fig. 9) from pre-EECO to early EECO. This is also associated with the most notable biotic change in the section, including the highest abundance of warm-water taxa and % planktic foraminifera (Fig. 12 d, e), increasing nannofossil and dinocyst diversity, and a long-term shift to more abundant and diverse angiosperm vegetation (Fig. 7). Declining SST from late EECO to post-EECO is mirrored with an increasing abundance of cool-water nannofossil and dinocyst taxa, although terrestrial vegetation shows little change in the post-EECO Heretaungan. It is not until the Bortonian that cooler temperatures are indicated by the rise in abundance of the Nothofagaceae, southern beech, family.

6.2 Early and middle Eocene sedimentation changes

Early Eocene extreme warming events are commonly linked with increased accumulation of terrigenous material on continental margins, including New Zealand, due to an enhanced hydrological cycle that promoted both chemical and physical weathering processes and transport of terrigenous sediment into adjacent basins (Dickens et al., 1997; Schmitz and Pujalte, 2007; Carmichael et al.,

731 2017). This is well-documented for the short-lived PETM, which is also associated with notable
732 changes in sedimentation patterns and marine primary productivity (Crouch et al., 2003; Nicolo et al.,
733 2007; Giusberti et al., 2016). Equivalent EECO records are sparse, making it difficult to compare the
734 climatic impacts on sedimentation between transient and long-term warming events. In New Zealand,
735 the Mead and Branch Stream (Fig. 1) records suggests similar changes in terrigenous delivery and
736 sedimentation occurred in the EECO to that documented for the PETM, with an increased component
737 of terrigenous-sourced clay during early Eocene CIEs, as well as in the EECO, and highest sediment
738 accumulation rates (SARs) during the EECO (Slotnick et al., 2012, 2015; Dallanave et al., 2014).

739 At mid-Waipara, SARs also appear to have increased at the base of the EECO (from ~4 to 10
740 m/Myr), peaked in the latest EECO (14 m/Myr), and then stabilised through the overlying post-EECO
741 Heretaungan (~10 m/Myr; Dallanave et al., 2016). However, SAR estimates are uncertain for the base
742 of the section due to limited exposure, and in the late Heretaungan due to likely erosion at the
743 overlying unconformity (~59 m). The SAR is generally much higher at Mead Stream (Dallanave et
744 al., 2014), despite the sediments being primarily pelagic carbonate and hemipelagic clays; background
745 SAR is 20 m/Myr and peak SAR in the EECO is 40–100 m/Myr at Mead Stream. This indicates that
746 the Eocene section at mid-Waipara is relatively condensed and that cryptic unconformities may be
747 present, which would distort the estimates of SAR.

748 Two other commonly used proxies for terrigenous input in marine sediments, the BIT index
749 and terrestrial palynomorph abundance (Fig. 12f), exhibit opposing trends in the lower part of the
750 early Eocene. This may be related to other factors influencing the BIT index, as discussed above
751 (section 5.3). However, the convergence of trends in the mid–late EECO and post-EECO Heretaungan
752 suggests that cooling is linked to increased terrigenous input in this section.

753 In this respect, the mid-Waipara record differs from Mead Stream, where a notable increase in
754 accumulation of terrigenous material is associated with the long-term EECO. This is further
755 emphasised by differences in thickness of the EECO at the two sections: 34 m at mid-Waipara versus
756 >100 m at Mead Stream (Supp. Information Fig. 2). Benthic foraminiferal assemblages indicate both
757 sections were deposited at bathyal depths in the early Eocene. Studies of the eastern Marlborough

758 pelagic succession (Reay, 1993; Hollis et al., 2005b) show that Mead Stream is the thickest, and most
759 distal, Paleocene–Eocene section of an oceanic carbonate ramp succession. Sections closer to the
760 paleo-shoreline are thinner, with major unconformities truncating the succession in this proximal area.
761 A similar relation may apply to Mead and mid-Waipara sections, with Mead being in a distal
762 depocenter for terrigenous weathering products in the EECO, whereas mid-Waipara represents a more
763 dynamic coastal setting, where climatic changes cause changes in sediment delivery pathways and
764 result in a more complex relationship between SAR and other indicators of terrigenous supply, sea
765 level change and climate.

766

767 *6.3 Early and middle Eocene changes in marine productivity and surface water conditions*

768 Marine microfossils can provide insight into surface productivity and nutrient availability.
769 Peridinioid dinocysts, predominantly heterotrophic dinoflagellates, make up <20% of the assemblage
770 in the lower–mid EECO, and the abundance peak (40%) in the late EECO is coincident with an
771 increase in the BIT index and terrestrial palynomorph abundance (Fig. 12f, g). Peridinioid abundance
772 is <30% of the assemblage in the post-EECO. The lowest peridinioid abundance is associated with the
773 negative CIEs and high SST (correlation r = 0.39, p <0.02 and r = -0.3, p <0.01, n = 43, with $\delta^{13}C$ and
774 TEX_{86}, respectively).

775 Several short-lived abundance peaks, up to 30%, of the genus *Homotryblium* in the early and
776 middle EECO (Fig. 12e) suggest the presence of seasonally elevated salinity levels and/or surface
777 water stratification (Frieling and Sluijs, 2018). *Homotryblium* is morphologically like the extant
778 euryhaline species *Polysphaeridium zoharyi*, which occurs in low–mid latitudes and is tolerant to
779 extreme salinities and shallow water depths (Edwards and Anderle, 1992; Reichart et al., 2004). Most
780 studies suggest *Homotryblium* has an affinity to hypersaline environments (Köthe, 1990; Pross and
781 Schmiedl, 2002), although there is a possibility the genus favoured low-salinity conditions (Dybkjær,
782 2004). Whilst super-abundant *Homotryblium* is commonly linked with lagoonal/restricted inner
783 marine settings (e.g., de Verteuil and Norris, 1996), benthic foraminiferal assemblages show the
784 Ashley Mudstone was deposited at bathyal depths. The *Homotryblium* peaks do not correlate with

785 inner neritic dinocyst increases (e.g., *Cordosphaeridium*, *Glaphyrocysta*; Fig. 7), suggesting the
786 surface water conditions that led to *Homotryblium* blooms were not restricted to a coastal setting but
787 extended into the Canterbury Basin. The EECO *Homotryblium* peaks correspond with high SST and
788 %$GDGT_{RS}$ values >30 (Fig. 12 b, c), and partly correlate with CIEs (#3 and #4) and peaks in warm-
789 water nannofossils (Figs. 12a, d). Elsewhere, high %$GDGT_{RS}$ values (>30) are seen in times of
790 elevated warmth (PETM and EECO) from the North Sea Basin, New Jersey margin and SW Pacific
791 sites that have coeval high abundances of epicystal Goniodomidae dinocysts, such as *Eocladopyxis,*
792 *Polysphaeridium* and *Homotryblium* (Sluijs and Brinkhuis, 2009; Inglis et al., 2015; Frieling and
793 Sluijs, 2018). In New Zealand, abundant *Homotryblium* is also noted in the EECO at Mead Stream
794 (Cooper, 2018) and Hampden Beach (Inglis et al., 2015).

795 While deciphering the influence of productivity on nannofossil assemblages is complicated by
796 the interconnectivity between temperature and nutrient availability (Agnini et al., 2007; Schneider et
797 al., 2011), some general observations indicate that surface productivity at mid-Waipara did not
798 increase in the EECO. Rather, the EECO is characterised by the replacement of one mesotrophic
799 genus, *Toweius*, with another, *Reticulofenestra*, which occurs in the late EECO and is coeval with the
800 peridinioid abundance peak and increasing BIT values and terrestrial palynomorph abundance (Fig.
801 12f, g). The combined abundance of *Toweius* and *Reticulofenestra* is lower in the EECO (average
802 46%) than it is below or above the EECO (average 65% and 55%, respectively).

803 At the oceanic bathyal Mead Stream, there is evidence for increased terrigenous-sourced clay
804 content and SARs in the EECO (Slotnick et al., 2012; Dallanave et al., 2015), but no clear signal of
805 enhanced marine surface productivity. A marked decline in radiolarian abundance and diversity, and
806 low diatom abundance, imply a decrease in biosiliceous productivity linked with the EECO (Hollis,
807 2006). Rather, assemblages characteristic of oligotrophic, possibly stratified, conditions prevailed.
808 Open ocean gonyaulacoid taxa dominate dinocyst assemblages in the EECO, and super-abundant
809 *Homotryblium* occurs in an interval corresponding with the J-event (EECO onset; Cooper, 2018).

810

811 *6.4 Early Eocene vegetation change*

In New Zealand, the most notable long-term vegetation shift in the early Eocene is the widespread abundance increase in Casuarinaceae pollen of *Myricipites harrisii* (Raine, 1984; Pocknall, 1990; Crouch and Brinkhuis, 2005). The precise timing is poorly constrained due to difficulties in accurately dating terrestrial sediments and correlation with well-calibrated marine sections (Morgans et al., 2004; Raine et al., 2009; Handley et al., 2011). The vegetation shift has been correlated with middle–late Waipawan, nannofossil Zone NP11 and dinocyst zone NZE3 (Crouch and Brinkhuis, 2005), but a direct link with Eocene climatic changes has not been made until this study.

Our results provide the clearest evidence to date that the Casuarinaceae increase is correlated with EECO warming. The increase in *M. harrisii* abundance is in the late Waipawan (Fig. 8), and corresponds with the warmest SST in the early EECO (Fig. 12b). Casuarinaceae remain frequent–abundant in the EECO, and whilst there is a gradual decline in abundance post-EECO, the duration of common–abundant *M. harrisii* continues at least 4–5 Myr above the EECO and into the middle Eocene Porangan Stage (Raine et al., 2009).

Pollen of *M. harrisii* is first seen in New Zealand and Australia in the early–middle Paleocene (Raine, 1984; Macphail et al., 1994; Contreras et al., 2014), but is relatively sparse until the early Eocene. Whilst *M. harrisii* is common or abundant in New Zealand in the early–middle Eocene, the southern Australia record is varied: high abundances occur in the Australo-Antarctic basins (e.g., Otway Basin) but not in Southeastern Australia (e.g., Gippsland Basin), where gymnosperm pollen remain abundant (Harris, 1965; Carpenter et al., 2012; Contreras et al., 2014; Holdgate et al., 2017). Casuarinaceae is a family characteristic of sclerophyllous, seasonally dry forests, but also includes the primitive genus *Gymnostoma*, a tropical–subtropical rainforest margin taxon adapted to low nutrient soils (Hill, 1994; Prider and Christophel, 2000; Steane et al., 2003). Fossil pollen of *Gymnostoma* and *Casuarina* are virtually indistinguishable, apart from the latter being generally larger (Kershaw, 1970). Whilst macrofossil evidence suggests *Gymnostoma* was common in the early Paleogene (Christophel, 1980; Hill, 1994; Greenwood and Christophel, 2005), the earliest macrofossil record of *Casuarina* is less clear, perhaps in the Eocene, but the oldest definitive macrofossils are Oligocene (Greenwood and Christophel, 2005; McGowran and Hill, 2015). The ecological interpretation of *M.*

839 *harrisii* is therefore complicated by the possibility that pollen was produced by *Gymnostoma* and
840 *Casuarina* plants.

841 A combination of causes may have led to the long-term increase in Casuarinaceae vegetation
842 linked with the EECO in New Zealand. Firstly, transient extreme warming at the PETM did not have
843 a notable effect on Casuarinaceae (Crouch and Brinkhuis, 2005), but longer-term warming associated
844 with the EECO may have allowed for vegetation change to occur and become established. At mid-
845 Waipara, EECO mean annual temperature (MAT) estimates have been calculated from spore and
846 pollen assemblages, which range from 17.1 ± 6.8°C (bioclimatic analysis) to 22.6 ± 1.4°C (co-
847 existence approach) in the EECO (Pancost et al., 2013). MAT estimates are lower than geochemical-
848 based SST proxies (Fig. 10; Hollis et al., 2019). Secondly, precipitation changes may have led to
849 conditions well-suited to Casuarinaceae. Hydrogen isotopes of plant biomarkers ($\delta D_{n\text{-alkane}}$) from the
850 Kumara-2 core (Fig. 1) show a general increase in the early Eocene, with highest values (-135‰)
851 coeval with the *M. harrisii* increase, perhaps suggesting a more seasonal climate or increasing aridity
852 (Handley et al., 2011). Moreover, long-term changes in temperature and precipitation patterns may
853 have led to changes in soil conditions more favourable for Casuarinaceae. Results from the Taranaki
854 Basin (Fig. 1) indicate enhanced chemical weathering in the early Eocene (Zone MH1), with
855 increased quartz-K-feldspar sediments and a decline in plagioclase-rich sediments (Higgs et al.,
856 submitted).

857

858 **7. Conclusions**

859 The early Paleogene succession at mid-Waipara River, Canterbury Basin, New Zealand, has
860 been the focus of several high-profile paleoclimate studies as the sediments contain good preservation
861 of microfossils and organic biomarkers. Here, we build on this previous work and undertake a
862 quantitative analysis of paleontological and multiproxy geochemical indicators of climate and
863 environmental change through the early–middle Eocene, with particular focus on the Early Eocene
864 Climatic Optimum (EECO).

865 The section spans the early Eocene (New Zealand Waipawan Stage) to middle Eocene (lower
866 Bortonian Stage), ~55.5–42.5 Ma, with a non-exposed interval in the lower Eocene (middle
867 Waipawan) and an unconformity, spanning ~3 Myr, in the middle Eocene (latest Heretaungan,
868 Porangan and earliest Bortonian Stages). The EECO corresponds with a ~33.5 m interval from late
869 Waipawan to the Mangaorapan/Heretaungan boundary, 49.27 Ma, in upper Chron C22n. The EECO
870 onset is not captured as it occurs in the non-exposed interval, but the termination is preserved and
871 corresponds to a sustained shift to lower TEX_{86} values and more positive bulk carbonate $\delta^{13}C$ values.
872 A series of six negative CIEs are identified in the EECO and tentatively correlated with named CIEs
873 in global benthic $\delta^{13}C$ compilations. These CIEs are found to be associated with high TEX_{86} values,
874 indicating that they represent hyperthermals.

875 The TEX_{86} record indicates that SST increased from the earliest Eocene to the early EECO,
876 by 7°C with the TEX_{86}^{H} calibration and by 12°C with the BAYSPAR calibration. Peak SST for the
877 EECO were 34°C (TEX_{86}^{H} calibration) and 36°C (BAYSPAR calibration). SST began to gradually
878 decline from the middle EECO (~51 Ma) and reached minimum values for the post-EECO
879 Heretaungan at ~47 Ma (27°C and 22°C, respectively). Similar average values are recorded for the
880 overlying Bortonian Stage, but with significant variation in SST estimates of 6–8°C. This SST record
881 is in good agreement with previous estimates from a lower resolution sample set using TEX_{86} and
882 planktic foraminiferal $\delta^{18}O$ and Mg/Ca ratios (Hollis et al., 2009, 2012; Creech et al., 2010).

883 We also find good agreement between the relative temperature trend for TEX_{86} and trends in
884 marine microfossil proxies for temperature, providing confidence that both approaches are useful
885 guides to past water temperature. Pronounced warming in the early EECO corresponds with the most
886 pronounced biotic changes in the section. This includes increased diversity in calcareous nannofossil
887 and dinocyst assemblages, the highest abundance of warm-water taxa and planktic foraminifera, and a
888 long-term shift to abundant and diverse angiosperm vegetation, primarily driven by a rise in
889 Casuarinaceae. Marine microfossils also offer a means to evaluate the inference drawn from
890 geochemical proxies that latitudinal temperature gradients were greatly reduced in the EECO. Our
891 provisional analysis of microfossil assemblages indicates the latitudinal temperature gradient between

mid- and low latitudes in the EECO was greater than that indicated by geochemical SST proxies. Further biogeographic studies of microfossil assemblages are needed to determine if it is possible to quantify these gradients.

There is no clear evidence for a notable increase in sedimentation rates or accumulation of terrigenous material associated with warmest temperatures of the EECO. This contrasts with that previously documented at the nearby oceanic carbonate Mead Stream section and may reflect different sediment delivery pathways and a more dynamic coastal mid-Waipara setting. Marine surface productivity does also not appear to have increased in the warmest part of the EECO, although superabundant *Homotryblium*, a euryhaline dinocyst genus, in the early and middle EECO suggest the presence of seasonally elevated salinity levels and/or stratified surface waters. In the late EECO, from ~50 Ma, combined proxies indicate declining temperatures correspond with an increase in cool-water marine taxa and contribution of terrigenous material into the Canterbury Basin, which continued into the post-EECO.

This multi-proxy study of the continental margin mid-Waipara River section shows the value of combining well-calibrated biological and geochemical records to better constrain and understand past warm climate states, and to provide a robust means to interrogate geochemical-based temperature proxies (Hollis et al., 2019).

Acknowledgements

Roger Tremain, Henry Gard and Sonja Bermudez (GNS Science) are thanked for sample preparation. This study was supported by the New Zealand Government's Strategic Science Investment Fund through the GNS Science Global Change through Time Programme. RDP and BDAN acknowledges the ERC for funding the Advanced Grant T-GRES and the NERC for funding SWEET. BDAN acknowledges additional funding through a Royal Society Tata University Research Fellowship. We thank the two anonymous reviewers for very constructive and helpful reviews, and the editor for his comments and proofreading.

Figures

1. Location of the mid-Waipara River section in northeast South Island (A), and early Eocene (50 Ma) paleogeographic reconstruction for the Southwest Pacific based on the paleomagnetic reference frame of Matthews et al. (2016) (B). Thick red line in (A) shows the position of Ashley Mudstone samples examined in this study. HB = Hampden Beach, KC = Kumara-2 core, TB = Taranaki Basin.

2. The early and middle Eocene timescale (GTS2014, after Gradstein et al. 2012; Ogg et al., 2014; NZGTS2015, after Raine et al., 2015) and global benthic foraminiferal isotope record (Cramer et al., 2009; recalibrated to GTS2014). The age of the Mangaorapan/Heretaungan boundary is recalibrated to Westerhold et al. (2017). Ages of calcareous nannofossil (NP) zone boundaries are based on Gradstein et al. (2012), with adjustments to Zones NP9 to NP14 after Hollis et al. (2019). The New Zealand dinocyst and spore/pollen zones are from Wilson et al. (1988) and Morgans et al. (2004); *C. col* = *Charlesdowniea coleothrypta*, *C. ed* = *Charlesdowniea edwardsii*, *M. pe* = *Membranophoridium perforatum*, *W. ec* = *Wilsonidium echinosuturatum*). Grey bands represent the position of the Paleocene–Eocene Thermal Maximum (PETM) and Early Eocene Climatic Optimum (EECO).

3. Summary of the mid-Waipara River lithological column (Ashley Mudstone), and ranges of biostratigraphic marker taxa and biozones in the early to middle Eocene. Also shown are the stratigraphic distribution of samples taken from the Ashley Mudstone for both the 2007 and 2012 collections, and planktic foraminiferal abundance (%). Thickened lines indicate intervals of common (>8%) abundance. Magnetostratigraphy from Dallanave et al. (2016), NP zones are calcareous nannofossil zones.

4. Variation in calcium carbonate ($CaCO_3$) content (a), and calcareous nannofossil preservation (b), diversity (c) and relative abundance of biogeographic indicator taxa (d) in the mid-Waipara River section. Preservation indicators include visually observed preservation (VOP, black line and markers)

and relative abundance of *Zygrhablithus bijugatus* (red line and markers), a species sensitive to dissolution. Diversity is indicated by taxon richness (black line and markers) and the Shannon diversity index (red line and markers). Relative abundance of cool- and warm-water calcareous nannofossil groups is shown, including selected cool (*Chiasmolithus* spp. and *Reticulofenestra daviesii*) and warm-water (*Discoaster* spp., *Spenolithus* spp., and *Coccolithus formosus*) taxa. Shaded intervals show the position of the Early Eocene Climatic Optimum (EECO, light grey) and the negative carbon isotope excursions (numbered 1 to 6, dark grey).

5. Variation in calcium carbonate ($CaCO_3$) content (a), bulk carbonate $\delta^{13}C$ (b), TEX_{86} (c), and BIT Index (d) for the early and middle Eocene in the mid-Waipara River section. Shaded intervals show the position of the Early Eocene Climatic Optimum (EECO, light grey) and the negative carbon isotope excursions (numbered 1 to 6, dark grey).

6. The mid-Waipara River bulk carbonate $\delta^{13}C$ and TEX_{86} records (b) compared with the benthic foraminiferal stable isotope compilation (a) for North Pacific ODP Site 1209 and South Atlantic ODP sites 1258, 1262 and 1263 of Westerhold et al. (2018), calibrated to the timescale of Westerhold et al. (2017). Grey band and dashed lines represent the Early Eocene Climatic Optimum (EECO) and carbon isotope excursions (CIEs). The six CIEs at mid-Waipara River are tentatively correlated with named CIEs as indicated.

7. The relative abundance of selected dinocyst species and genera from the early and middle Eocene in the mid-Waipara River section. Gonyaulacoid dinocysts are shown in dark grey; peridinioid dinocysts in light grey. The relative abundances of total peridinioid dinocysts and climate indicator taxa are also shown. Shaded bands represent the Early Eocene Climatic Optimum (EECO, light grey) and the negative carbon isotope excursions (dark grey).

970 **8.** The relative abundance of total terrestrial palynomorphs, selected spore and pollen species and
971 genera, and relative proportions of spore, gymnosperm and angiosperm groups from the early and
972 middle Eocene in the mid-Waipara River section. Shaded bands represent the Early Eocene Climatic
973 Optimum (EECO, light grey) and the negative carbon isotope excursions (dark grey).

974

975 **9.** Temperature variation and associated parameters in the early and middle Eocene at mid-Waipara
976 River section: sea surface temperature (SST) record using BAYSPAR and TEX_{86}^{H} calibrations, with
977 95% confidence band for BAYSPAR (a), relative temperature change of SST (BAYSPAR and
978 TEX_{86}^{H}) (b), and $\%GDGT_{RS}$ (c). Shaded bands represent the Early Eocene Climatic Optimum (EECO,
979 light grey) and the negative carbon isotope excursions (dark grey).

980

981 **10.** Summary of available isoGDGT- and foraminifera-based SST estimates from the early and middle
982 Eocene at mid-Waipara River, calibrated to the timescale of Westerhold et al. (2017). SSTs are
983 derived from TEX_{86} using BAYSPAR (this study) and TEX_{86}^{H} calibrations (this study and Hollis et
984 al., 2012). Foraminifera-based SST estimates are from Mg/Ca ratios and $\delta^{18}O$ values of the mixed
985 layer planktic genus *Morozovella* (Hollis et al., 2012, 2019). SST derived from the TEX_{86}^{H} and
986 BAYSPAR calibrations are warmer in some intervals than SST calculated from mixed layer
987 foraminifera (Mg/Ca ratios and $\delta^{18}O$ values), and this wider variation in $\delta^{18}O$-based SST is thought to
988 reflect diagenetic effects (Hollis et al., 2012). Error bars are ± 2.5°C TEX_{86}^{H} and 1 sigma for Mg/Ca
989 and $\delta^{18}O$; 95% confidence interval for BAYSPAR is shaded light blue. Shaded bands represent the
990 Early Eocene Climatic Optimum (EECO, light grey) and negative carbon isotope excursions (dark
991 grey).

992 **11.** The relative abundance of key calcareous nannofossil warm-water and cool-water taxa and genera
993 from selected subtropical (Site 1210, Shatsky Rise, Northwest Pacific Ocean), temperate (Site 762,
994 Exmouth Plateau, Indian Ocean; mid-Waipara River, Canterbury Basin; Site 277, Campbell Plateau),
995 and polar (Site 1135, Kerguelen Plateau, Southern Indian Ocean) provinces. Data for sites 762, 1135

and 1210 are from Schneider et al. (2011). Data are recalibrated to Gradstein et al. (2012). Sites are shown on a paleogeographic reconstruction for the early Eocene, using the same reference frame as in Fig. 1 (Matthews et al., 2016). The shaded band represents the Early Eocene Climatic Optimum (EECO).

12. Summary of climate and environmental proxies for the mid-Waipara River section, plotted against age (Westerhold et al., 2017). Bulk carbonate $\delta^{13}C$ record (a), TEX_{86}-derived SST based on BAYSPAR and TEX_{86}^{H} calibrations (b), % Red Sea GDGTs (c), calcareous nannofossil warm- and cool-water groups and % planktic foraminifera (d), dinocyst warm- and cooler-water groups (e), BIT index and % terrestrial palynomorphs (f), and calcareous nannofossil taxa and dinocyst peridinioids thought to be surface productivity indicators (g). Shaded bands represent the Early Eocene Climatic Optimum (EECO, light grey) and negative carbon isotope excursions (dark grey).

References

Agnini, C., Fornaciari, E., Rio, D., Tateo, F., Backman, J., Giusberti, L., 2007. Responses of calcareous nannofossil assemblages, mineralogy and geochemistry to the environmental perturbations across the Paleocene/Eocene boundary in the Venetian Pre-Alps. Marine Micropaleontology 63, 19–38, doi: 10.1016/j.marmicro.2006.10.002.

Agnini, C., Fornaciari, E., Raffi, I., Catanzariti, R., Pälike, H., Backman, J., et al., 2014. Biozonation and biochronology of Paleogene calcareous nannofossils from low and middle latitudes. Newsletters on Stratigraphy 47, 131–181.

Anagnostou, E., John, E.H., Edgar, K.M., Foster, G., Ridgwell, A., Inglis, G.N., Pancost, R.D., Lunt, D.J., Pearson, P.N., 2016. Changing atmospheric CO_2 concentration was the primary driver of early Cenozoic climate. Nature, doi:10.1038/nautre17423.

Aubry, M.-P., 1991. Sequence stratigraphy: Eustasy or tectonic imprint? Journal of Geophysical Research 96, 6641–6679, doi: 10.1029/90JB01204.

Awad, W.K., Oboh-Ikuenobe, F.E., 2016. Early Paleogene dinoflagellate cysts from ODP Hole 959D, Côte d'Ivoire-Ghana Transform Margin, West Africa: new species, biostratigraphy and paleoenvironmental implications. Journal of African Earth Sciences 123, 123–144.

Backman, J., 1986. Late Paleocene to middle Eocene calcareous nannofossil biochronology from the Shatsky Rise, Walvis Ridge and Italy. Palaeogeography, Palaeoclimatology, Palaeoecology 57, 43–59.

Barnet, J.S.K., Littler, K., Westerhold, T., Kroon, D., Leng, M.J., Bailey, I., Röhl, U., Zachos, J.C., 2019. A high-fidelity benthic stable isotope record of Late Cretaceous–Early Eocene climate change and carbon-cycling. Paleoceanography and Paleoclimatology 34, 672–679. https://doi.org/10.1029/2019PA003556.

Beerling, D.J., Royer, D.L., 2011. Convergent Cenozoic CO_2 history. Nature Geosciences 4, 418–420.

Bijl, P.K., Schouten, S., Sluijs, A., Reichart, G.-J., Zachos, J.C., Brinkhuis, H., 2009. Early Paleogene temperature evolution of the southwest Pacific Ocean. Nature 461, 776–779.

Bijl, P.K., Pross. J., Warnaar, J., Stickley, C., Huber, M., Guerstein, R., Houben, A.J.P., Sluijs, A., Visscher, H., Brinkhuis, H., 2011. Environmental forcings of Paleogene Southern Ocean dinoflagellate biostratigraphy. Paleoceanography 26, PA1202, doi:10.1029/2009PA001905.

Bijl, P.K., Sluijs, A., Brinkhuis, H., 2013a. A magneto- and chemostratigraphically calibrated dinoflagellate cyst zonation of the early Paleogene South Pacific Ocean. Earth-Science Reviews 124, 1–31.

Bijl, P.K., Bendle, J., Boharty, S., Pross. J., Schouten, S., Tauxe, L., Stickley, C., McKay, R., Röhl, U., Olney, M., Sluijs, A., Escutia, C., Brinkhuis, H., and Expedition 318 Scientists, 2013b. Eocene cooling linked to early flow across the Tasmanian Gateway. Proceedings of the national Academy of Science U.S.A 110, 9645–9650.

Bown, P. R., 1998. Calcareous Nannofossil Biostratigraphy. Cambridge University. 315 p.

Bown, P. R., 2005. Paleogene calcareous nannofossils from the Kilwa and Lind areas of coastal Tanzania (Tanzania Drilling Project 2003–4). Journal of Nannoplankton Research 27, 21–95.

Bown, P. R., Young, J. R., 1998. Techniques. *In* Bown, P. R. (Ed.), Calcareous Nannofossil Biostratigraphy. London: Kluwer Academic Publishers, 16–28.

Boudreau, B., Middelburg, J., Sluijs, A., van der Ploeg, R., 2019. Secular variations in the carbonate chemistry of the oceans over the Cenozoic. Earth Planetary Science Letters 512, 194–206.

Bralower, T. J., 2002. Evidence of surface water oligotrophy during the Paleocene–Eocene thermal maximum: Nannofossil assemblage data from Ocean Drilling Program Site 690, Maud Rise, Weddell Sea. Paleoceanography 17, doi: 10.1029/2001pa000662.

Brinkhuis, H., 1994. Late Eocene to Early Oligocene dinoflagellate cysts from the Priabonian type-area (northeast Italy): biostratigraphy and paleoenvironmental interpretation. Palaeogeography, Palaeoclimatology, Palaeoecology 107, 121–163.

Carlson, H., Caballero, R., 2017. Atmospheric circulation and hydroclimate impacts of alternative warming scenarios for the Eocene. Climates of the Past 13, 1037–1048.

Carmichael, M., Inglis, G., Badger, M., Naafs, B.D., Behrooz, L., Remmelzwaal, S., Monteiro, F., Rohrssen, M., Farnsworth, A., Buss, H., Dickson, A., Valdes, P., Lunt, D., Pancost, R.D., 2017. Hydrological and associated biogeochemical consequences of rapid global warming during the Paleocene–Eocene Thermal Maximum. Global and Planetary Change 157, 114–138.

Carpenter, R.J., Jordan, G.J., Macphail, M.K., Hill, R.S., 2012: Near-tropical Early Eocene terrestrial temperatures at the Australo-Antarctic margin, western Tasmania. Geology 40, 267–270.

Christophel, D.C., 1980: Occurrence of *Casuarina* megafossils in the Tertiary of South-eastern Australia. Australian Journal of Botany 27, 249–259.

Contreras, L., Pross, J., Bijl, P.K., O'Hara, R.B., Raine, J.I., Sluijs, A., Brinkhuis, H., 2014: Southern high-latitude terrestrial climate change during the Paleocene–Eocene derived from a marine pollen record (ODP Site 1172, East Tasman Plateau). Climate of the Past 10, 1401–1420.

Cooper, R.A. (editor), 2004. The New Zealand Geological Timescale. Institute of Geological and Nuclear Sciences Monograph 22. 284p.

Cooper, T.F., 2018. Early Eocene palynology from Mead Stream, New Zealand. Master of Science (Geology) thesis, Victoria University of Wellington, December 2017.

Cramer, B., Wright, J.D., Kent, D.V., Aubry, M.-P., 2003. Orbital climate forcing of $\delta^{13}C$ excursions in the late Paleocene–early Eocene. Paleoceanography 18, 1097, doi:10.1029/2003PA000909.

Cramer, B., Toggweiler, J.R., Wright, J.D., Katz, M.E., Miller, K.G., 2009. Ocean overturning since the Late Cretaceous: Inferences from a new benthic foraminiferal isotope compilation. Paleoceanography 24, PA4216, doi:10.1029/2008PA001683.

Cramwinckel, M.J., Huber, M., Kocken, I., Agnini, C., Bijl, P., Boharty, S., Frieling, J., Goldner, A., Hilgen, F., Kip, E., Peterse, F., van der Ploeg, R., Röhl, U., Schouten, S., Sluijs, A., 2018. Synchronous tropical and polar temperature evolution in the Eocene. Nature, doi.org/10.1038.s41586-018-0272-2.

Creech, J.B., Baker, J., Hollis, C.J., Morgans, H.E.G., Smith, E., 2010. Eocene sea temperatures for the mid-latitude southwest Pacific from Mg/Ca ratios in planktonic and benthic foraminfera. Earth and Planetary Science Letters 299, 483–495.

Crouch, E.M., Brinkhuis, H., 2005: Environmental change across the Paleocene–Eocene transition from eastern New Zealand: a marine palynological approach. Marine Micropaleontology 56, 138–160.

Crouch, E.M., Heilmann-Clausen, C., Brinkhuis, H., Morgans, H., Rogers, K., Egger, H., Schmitz, B., 2001. Global dinoflagellate events associated with the late Paleocene thermal maximum. Geology 29, 315–318.

Crouch, E.M., Brinkhuis, H., Visscher, H., Adatte, T., Bolle, M.-P., 2003. Late Paleocene–early Eocene dinoflagellate cyst records from the Tethys: further observations on the global distribution of *Apectodinium*. Geological Society of America Special Paper 369, 113–131.

Crouch, E.M., Dickens, G.R., Brinkhuis, H., Aubry, M.-P., Hollis, C.J., Rogers, K.M., Visscher, H., 2003. The *Apectodinium* acme and terrestrial discharge during the Paleocene–Eocene thermal maximum: new palynological, geochemical and calcareous nannoplankton observations at Tawanui, New Zealand. Palaeogeography, Palaeoclimatology, Palaeoecology 194, 387–403.

Dale, B., 1996. Dinoflagellate cyst ecology: modelling and geological applications. In: Jansonius, J, McGregor, D.C. (Eds.), Palynology: Principles and Applications. AASP Foundation, 1249–1275.

Dallanave, E., Agnini, C., Bachtadse, V., Muttoni, G., Crampton, J.S., Strong, C.P., Hines, B.R., Hollis, C.J., Slotnick, B.S., 2015. Early to middle Eocene magneto-biochronology of the southwest Pacific Ocean and climate influence on sedimentation: Insights from the Mead Stream section, New Zealand. Geological Society of America Bulletin 127, 643–660.

Dallanave, E., Bachtadse, V., Crouch, E.M., Tauxe, L., Shepherd, C.L., Morgans, H.E.G., Hollis, C.J., Hines, B.R., Sugisaki, S., 2016. Constraining early to middle Eocene climate evolution of the southwest Pacific and Southern ocean. Earth and Planetary Science Letters 433, 380–392.

De Jonge, C., Hopmans, E.C., Stadnitskaia, A., Rijpstra, W.I.C., Hofland, R., Tegelaar, E., Sinninghe Damsté, J.S., 2013: Identification of novel penta- and hexamethylated branched glycerol dialkyl glycerol tetraethers in peat using HPLC–MS^2, GC–MS and GC–SMB-MS. Organic Geochemistry 54, 78-82, doi: 10.1016/j.orggeochem.2012.10.004.

De Jonge, C., Hopmans, E.C., Zell, C.I., Kim, J.-H., Schouten, S., Sinninghe Damsté, J.S., 2014a: Occurrence and abundance of 6-methyl branched glycerol dialkyl glycerol tetraethers in soils: implications for palaeoclimate reconstruction. Geochimica et Cosmochimica Acta 141, 97-112, doi: 10.1016/j.gca.2014.06.013.

De Jonge, C., Stadnitskaia, A., Hopmans, E.C., Cherkashov, G., Fedotov, A., Sinninghe Damsté, J.S., 2014b. In situ produced branched glycerol dialkyl glycerol tetraethers in suspended particulate matter from the Yenisei River, Eastern Siberia. Geochimica et Cosmochimica Acta 125, 476-491.

De Vernal, A., Eynaud, F., Henry, M., Hillaire-Marcel, C., Londeix, L., Mangin, S., Matthiessen, J., Marret, F., Radi, T., Rochon, A., Solignac, S., Turon, J., 2005. Reconstruction of sea-surface conditions at middle to high latitudes of the Northern Hemisphere during the Last Glacial maximum (LGM) based on dinoflagellate cyst assemblages. Quaternary Science Reviews 24, 897–924.

De Verteuil, L., Norris, G., 1996. Middle to upper Miocene *Geonettia clinae*, an opportunistic coastal embayment dinoflagellate of the *Homotryblium* complex. Micropaleontology 42, 263–284.

Dickens, G.R., Castillo, M., Walker, J., 1997. A blast of gas in the latest Paleocene: simulating first-order effects of massive dissociation of oceanic methane hydrate. Geology 25, 259–262.

Dunkley Jones, T., Bown, P. R., Pearson, P. N., 2009. Exceptionally well preserved upper Eocene to lower Oligocene calcareous nannofossils (Prymnesiophyceae) from the Oande Formation (Kilwa Group), Tanzania. Journal of Systematic Paleontology 7, 359–411.

Dybkjær, K., 2004. Morphological and abundance variations in *Homotryblium*-cyst assemblages related to depositional environments; uppermost Oligocene–Lower Miocene, Jylland, Denmark. Palaeogeography, Palaeoclimatology, Palaeoecology 206, 41–58.

Edwards, L.E., Andrele, V., 1992. Distribution of selected dinoflagellate cysts in modern marine sediments. *In*: Head, M., Wrenn, J. (eds.), Neogene and Quaternary Dinoflagellate Cysts and Acritarchs. American Association of Stratigraphic Palynologists, Texas, p. 250–273.

Evans, D., Sagoo, N., Renema, W., Cotton, L., Müller, W., Todd, J., Saraswati, P.K., Stassen, P., Ziegler, M., Pearson, P., Valdes, P., Affek, H., 2018. Eocene greenhouse climate revealed by coupled clumped isotope-Mg/Ca thermometry. Proceedings of the National Academy of Sciences, 10.1073/pnas.1714744115.

Frieling, J., Iakovleva, A., Reichart, G.-J., Aleksandrova, G., Gnibidenko, Z., Schouten, S., Sluijs, A., 2014. Paleocene–Eocene warming and biotic response in the epicontinental West Siberian Sea. Geology 42, 767–770.

Frieling, J., Sluijs, A., 2018. Towards quantitative environmental reconstructions from ancient non-analogue microfossil assemblages: Ecological preferences of Paleocene–Eocene dinoflagellates. Earth-Science Reviews 185, 956–973.

Giusberti, L., Boscolo Galazzo, F., Thomas, E., 2016. Variability in climate and productivity during the Paleocene–Eocene Thermal Maximum in the western Tethys (Forada section). Climate of the Past 12, 213–240.

Gradstein, F. M., Ogg, J. G., Schmitz, M., Ogg, G., 2012. The Geologic Time Scale 2012. Elsevier, 1176 p.

Greenwood, D.R., Christophel, D 2005: The origins and Tertiary history of Austrlian "tropical" rainforests. *In*: Bermingham, E., Dick, C., Moritz, C. (eds.), Tropical Rainforests: past, present and future. University of Chicago Press, p. 336–373.

Guasti, E., Kouwenhoven, T.J., Brinkhuis, H., Speijer, R.P., 2005. Paleocene sea-level and productivity changes at the southern Tethyan margin (El Kef, Tunisia). Marine Micropaleontology 55, 1–17.

Handley, L, Crouch, E.M., Pancost, R.D., 2011: A New Zealand record of sea level rise and environmental change during the Paleocene–Eocene Thermal Maximum. Palaeogeography, Palaeoclimatology, Palaeoecology 305, 185–200.

Haq, B. U., 1981. Paleogene paleoceanography: early Cenozoic oceans revisited: Oceanologica Acta 4, supplement, 71-82.

Haq, B. U., Premoli-Silva, I., Lohmann, G.P., 1977. Calcareous plankton paleobiosgeographc evidence for major climatic fluctuations in the early Cenozoic Atlantic Ocean. Journal of Geohpysical Research 82, 3861–3876.

Harris, W.K., 1965: Basal Tertiary microflora from the Princetown area, Victoria, Australia. Palaeontographica Abt. B 115, 75–106.

Hayward, B.W., 1986. A guide to paleoenvironmental assessment using New Zealand Cenozoic foraminiferal faunas. New Zealand Geological Survey Report PAL 109. 73 p.

Hayward, B.W., Grenfell, H., Sabaa, A.T., Neil, H., Buzas, M., 2010. Recent New Zealand deep-water benthic foraminfiera: taxonomy, ecologic distribution, biogeography, and use in paleoenvironmental assessment. GNS Science Monograph 26. 363 p.

Hennissen, J., Head, M., Schepper, S., Groenveld, J., 2017. Dinoflagellate cyst paleoecology during Pliocene–Pleistocene climatic transition in the North Atlantic. Palaeogeography, Palaeoclimatology, Palaeoecology 470, 81–108.

Hernández-Sánchez, M.T., Woodward, E.M.S., Taylor, K.W.R., Henderson, G.M., Pancost, R.D., 2014: Variations in GDGT distributions through the water column in the South East Atlantic Ocean. Geochimica et Cosmochimica Acta 132, 337-348, doi: 10.1016/j.gca.2014.02.009.

Higgs, K.E., Munday, S., Forbes, A., Crouch, E., Sagar, M., submitted. A geochemical and biostratigraphic approach to investigating regional changes in sandstone composition through the Paleocene–Eocene, Taranaki Basin, New Zealand. Geological Magazine.

Hill, R.S., 1994: The history of selected Australian taxa. *In*: Hill, R.S. (ed.), History of the Australian vegetation: Cretaceous to Recent. Cambridge University Press, p. 390–419.

Hines, B.R., Hollis, C.J., Atkins, C.B., Baker, J.A., Morgans, H.E.G., Strong, C.P., 2017. Reduction of oceanic temperature gradients in the early Eocene Southwest Pacific Ocean. Palaeogeography, Palaeoclimatology, Palaeoecology 475, 41–54.

Holdgate, G.R., Sluiter, I.R.K., Taglieri, J., 2017: Eocene–Oligocene coals of the Gippsland and Australo-Antarctic basins - paleoclimatic and paleogeographic context and implications for earliest Cenozoic glaciations. Palaeogeography, Palaeoclimatology, Palaeoecology 472, 236–255.

Hollis, C.J., 2006. Radiolarian turnover through the Paleocene–Eocene transition, Mead Stream, New Zealand. Eclogae geol. Helv. 99 Supplement 1, S79–S99.

Hollis, C.J., Dickens, G.R., Field, B., Jones, C.M., Strong, C.P., 2005a. The Paleocene–Eocene transition at Mead Stream, New Zealand: a southern Pacific record of early Cenozoic global change. Palaeogeography, Palaeoclimatology, Palaeoecology 215, 313–343.

Hollis, C.J., Field, B., Jones, C.M., Wilson, G.J., Dickens, G.R., 2005b. Biostratigraphy and carbon isotope stratigraphy of uppermost Cretaceous–lower Cenozoic Muzzle Group in middle Clarence valley, New Zealand. Journal of the Royal Society of New Zealand 35, 345–383.

Hollis, C.J., Handley, L., Crouch, E.M., Morgans, H.E.G., Baker, J.A., Creech, J.B., Collins, K.S., Gibbs, S., Huber, M., Schouten, S., Pancost, R.D., Zachos, J.C., 2009. Tropical sea temperatures in the high-latitude South Pacific during the Eocene. Geology 37, 99–102.

Hollis, C.J., Taylor, K.W.R., Handley, L., Pancost, R.D., Huber, M., Creech, J.B., Hines, B.R., Crouch, E.M., Morgans, H.E.G., Crampton, J.S., Gibbs, S., Pearson, P.N., Zachos, J.C., 2012. Early Paleogene temperature history of the Southwest Pacific Ocean: Reconciling proxies and models. Earth and Planetary Science Letters 349-350, 53–66.

Hollis, C.J., Tayler, M.S., Andrew, B,, Taylor, K.W., Lurcock, P., Bijl, P.B., Kulhanek, D.K., Crouch, E.M., Nelson, C.S., Pancost, R.D., Huber, M., Wilson, G.S., Ventura, G.T., Crampton, J.S., Schiøler, P., Phillips, A., 2014. Organic-rich sedimentation in the South Pacific Ocean associated with Late Paleocene slimatic cooling. Earth-Science Reviews 134, 81–97.

Hollis, C.J., Hines, B.R., Littler, K., Villasante-Marcos, V., Kulhanek, D.K., Strong, C.P., Zachos, J.C., Eggins, S.M., Northcote, L., Phillips, A., 2015. The Paleocene–Eocene Thermal maximum at DSDP Site 277, Campbell Plateau, southern Pacific Ocean. Climate of the Past 11, 1009–1025.

Hollis, C.J., Dunkley Jones, T., Anagnostou, E., Bijl, P., Cramwinckel, M., Edgar, K, et al. 2019. The DeepMIP contribution to PMIP4: methodologies for selection, compilations and analysis of latest Paleocene and early Eocene climate proxy data. Geoscientific Model Devlopment, https://doi.org/10.5194/gmd-2018-309.

Hopmans, E.C., Schouten, S., Sinninghe Damsté, J.S., 2016: The effect of improved chromatography on GDGT-based palaeoproxies. Organic Geochemistry 93, 1-6, doi: 10.1016/j.orggeochem.2015.12.006.

Hopmans, E.C., Weijers, J.W.H., Schefuß, E., Herfort, L., Sinninghe Damsté, J.S., Schouten, S., 2004: A novel proxy for terrestrial organic matter in sediments based on branched and isoprenoid tetraether lipids. Earth and Planetary Science Letters 224, 107-116.

Huber, M., Nof, D., 2006. The ocean circulation in the southern hemisphere and its climatic impacts in the Eocene. Palaeogeography, Palaeoclimatology, Palaeoecology 231, 9–28.

Huber, M., Caballero, R., 2011. The early Eocene equable climate problem revisited. Climate of the Past 7, 603–633.

Huck, C.E., van de Flierdt, T., Boharty, S.M., Hammond, S.J., 2017. Antarctic climate, Southern Ocean circulation patterns, and deep water formation during the Eocene. Palaeoceanography 32, 674–691.

Iakovleva, A.I., Brinkhuis, H., Cavagnetto, C., 2001. Late Paleocene–Early Eocene dinoflagellate cysts from the Turgay Strait, Kazakhstan; correlations across ancient seaways. Palaeogeography, Palaeoclimatology, Palaeoecology 172, 243–268.

Iakovleva, A.I., Heilmann-Clausen, C., 2007. *Wilsonidium pechoricum* new species – a new dinoflagellate species with unusual asymmetry from the Paleocene/Eocene transition. Journal of Paleontology 8, 1020–1030.

Inglis, G.N., Farnsworth, A., Lunt, D., Foster, G.L., Hollis, C.J., Pagani, M., Jardine, P.E., et al., 2015: Descent toward the Icehouse: Eocene sea surface cooling inferred from GDGT distributions. Paleoceanography 29 doi: 10.1002/2014PA002723.

Jiang, S., Wise, S.W., 2009. Distinguishing the influence of diagenesis on the paleoecological reconstruction of nannoplankton across the Paleocene/Eocene Thermal Maximum: an example from the Kerguelen Plateau, southern Indian Ocean. Marine Micropaleontology 72, 49–59.

Kershaw, A.P., 1970. Pollen morphological variation within the Casuarinaceae. Pollen et Spores 12, 145–161.

Kim, J.-H., van der Meer, J., Schouten, S., Helmke, P., Willmott, V., Sangiorgi, F., Koç, N., et al., 2010. New indices and calibrations derived from the distribution of crenarchaeal isoprenoid tetraether lipids: Implications for past sea surface temperature reconstructions. Geochimica et Cosmochimica Acta 74, 4639-4654, doi: 10.1016/j.gca.2010.05.027.

Kirtland Turner, S., Sexton, P.F., Charles, C.D., Norris, R.D., 2014. Persistence of carbon release events through the peak of early Eocene global warmth. Nature Geoscience 7, 748–751.

Köthe, A., 1990. Paleogene dinoflagellates from northwest Germany: biostratigraphy and paleoenvironment. Geol. Jahrb. A 118, 3–111.
Lauretano, V., Littler, K., Polling, M., Zachos, J.C., Lourens, L.J., 2015. Frequency, magnitude and character of hyperthermal events at the onset of the Early Eocene Climatic Optimum. Climate of the Past 11, 1313–1324.
Lauretano, V., Hilgen, F.J., Zachos, J.C., Lourens, L.J., 2016. Astronomically tuned age model for the early Eocene carbon isotope events: A new high resolution $\delta^{13}C_{benthic}$ record of ODP Site 1263 between ~49 and ~54 Ma. Newsletters on Stratigraphy 49, 383–400.
Lauretano, V., Zachos, J.C., Lourens, L.J., 2018. Orbitally paced carbon and deep-sea temperature changes at the peak of the Early Eocene Climatic Optimum. Paleoceanography and Paleoclimatology 33, 1050–1065, doi: 10.1029/2018PA003422.
Littler, K., Röhl, U., Westerhold, T., Zachos, J.C., 2014. A high-resolution benthic stable-isotope record for the South Atlantic: Implications for orbital-scale changes in late Paleocene–Early Eocene climate and carbon cycling. Earth and Planetary Science Letters 401, 18–30.
Lunt, D.J., Dunkley Jones, T., Heinemann, M., Huber, M., LeGrande, A., Winguth, A., Loptson, C., Marotzke, J., Roberts, C.D., Tindall, J., Valdes, P., Winguth, C., 2012. A model-data comparison for a multi-model ensemble of ealy Eocene atmosphere-ocean simulations: EoMIP. Climate of the Past 8, 1717–1736.
Lunt, D.J., Huber, M., Anagnostou, E., Baatsen, M., Caballero, R.m DeConto, R., Dijkstra, H., Donnadieu, Y., Evans, D., et al., 2017. The DeepMIP contribution to PMIP4: experimental design for model simulations of the EECO, PETM and pre-PETM (version 1.0). Geoscientific Model Devlopment 10, 889–901.
Macphail, M.K., Alley, N.F., Truswell, E.M., Sluiter, I.R.K., 1994: Early Tertiary vegetation: evidence from spores and pollen. *In*: Hill, R.S. (ed.), History of the Australian vegetation: Cretaceous to Recent. Cambridge University Press, p. 189–261.
Martini, E., 1971. Standard Tertiary and Quaternary calcareous nannoplankton zonation. Paper presented at the Proceedings of the Second Planktonic Conference, Roma.
Matthews, K., Maloney, K., Zahirovic, S., Williams, S., Seton, M., Müller, D., 2016. Global plate boundary evolution and kinematics since the late Paleozoic. Global and Planetary Change 146, 226–250.
McGowran, B., Hill, R.S., 2015: Cenozoic climate shifts in southern Australia. Transactions of the Royal Society of South Australia 139, 19–37.
McIntyre, A., Bé, A.W.H., 1967. Modern Coccolithophoridae of the Atlantic Ocean. I. Placoliths and cyrtoliths. Deep Sea Research 14, 561–597.
Morgans, H.E.G., Beu, A.G., Cooper, R.A., Crouch, E.M, Hollis, C.J., Jones, C.M., Raine, J.I., Strong, C.P., Wilson, G.J., Wilson, G.S., 2004: Chapter 11, Paleogene (Dannevirke, Arnold and Landon Series). *In*: Cooper, R.A. (ed.), The New Zealand Geological Timescale. Institute of Geological and Nuclear Sciences Monograph 22, p. 125–163.
Morgans, H.E.G., Jones, C., Crouch, E.M, Field, B.D., Raine, J.I., Strong, C.P., Wilson, G.J., 2005. Upper Cretaceous to Eocene stratigraphy and sample collections, mid-Waipara River, North Canterbury. Institute of Geological and Nuclear Sciences report 2003/08. 101p.
Naafs, B.D.A., Pancost, R.D., 2016. Sea-surface temperature evolution across Aptian Oceanic Anoxic Event 1a. Geology 44, 959-962, doi: 10.1130/G38575.1.
Naafs, B.D.A., Gallego-Sala, A.V., Inglis, G.N., Pancost, R.D., 2017a. Refining the global branched glycerol dialkyl glycerol tetraether (brGDGT) soil temperature calibration. Organic Geochemistry 106, 48-56, doi: 10.1016/j.orggeochem.2017.01.009.
Naafs, B.D.A., Inglis, G.N., Zheng, Y., Amesbury, M.J., Biester, H., Bindler, R., Blewett, J., et al., 2017b. Introducing global peat-specific temperature and pH calibrations based on brGDGT bacterial lipids. Geochimica et Cosmochimica Acta 208, 285-301, doi: 10.1016/j.gca.2017.01.038.
Naafs, B.D.A., Rohrssen, M., Inglis, G., Lähteenoja, O., Feakins, S., Collinson, M., Kennedy, E., Singh, P., Lunt, D., Pancost, R.D., 2018. High temperatures in the terrestrial mid-latitudes during the early Paleogene. Nature Geoscience 11, 766–771, doi:10.1038/s41561-018-0199-0.
Nicolo, M.J., Dickens, G.R., Hollis, C.J., Zachos, J.C., 2007. Multiple early Eocene hyperthermals: Their sedimentary expression on the New Zealand continental margin and in the deep sea. Geology 35, 699–702.
O'Brien, C., Robinson, S., Pancost, R., Sinninghe Damsté, J., Schouten, S., Lunt, D., Alsenz, H., Bornemann, A., Bottini, C., Brassell, S., Farnsworth, A., Forster, A., Huber, B., Inglis, G., Jenkyns, H., Linnert, C., Littler, K., Markwick, P., McAnena, A., Mutterlose, J., Naafs, B.D.A., Püttmann, W., Sluijs, A., van Helmond, N.A.G.M., Vellekoop, J., Wagner, T., Wrobel, N., 2017. Cretaceous sea-surface temperature evolution: Constraints from TEX_{86} and planktonic foraminiferal oxygen isotopes. Earth-Science Reviews 172, 224-247, doi: 10.1016/j.earscirev.2017.07.012.
Okado, H., Honjo, S., 1973. The distribution of oceanic coccolithophorids in the Pacific. Deep Sea Research 20, 355–374.

Pälike, H., Lyle, M. (editors), 2010. Methods (Expedition 320/321 Scientists), *In* Proceedings of the Integrated Ocean Drilling Program, 320/321.
Pancost, R.D., Taylor, K., Inglis, G.N., Kennedy, E.M., Handley, L., Hollis, C.J., Crouch, E.M., Pross, J., Huber, M., Schouten, S., Pearson, P.N., Morgans, H.E.G., Raine, J.I., 2013. Early Paleogene evolution of terrestrial climate in the SW Pacific, Southern New Zealand. Geochemistry, Geophysics, Geosystems 14, doi:10.1002/2013GC004935.
Pearson, P.N., van Dongen, B., Nicholas, C.J., Pancost, R.D., Schouten, S., Singano, J., Wade, B., 2007. Stable warm tropical climate throug the Eocene Epoch. Geology 35, 211–214.
Perch-Nielsen, K., 1985. Cenozoic calcareous nannofossils. *In* Bolli, H., Perch-Nielsen, K., et al. (eds.), Plankton Stratigraphy (pp. 427–554). New York: Cambridge University Press.
Pocknall, D.T., 1990: Palynological evidence for the early and middle Eocene vegetation and climate history of New Zealand. Review of Palaeobotany and Palynology 65, 57–69.
Prasad, V., Garg, R., Khowaja-Ateequzzaman, Singh, I.B., Joachimski, M., 2006. *Apectodinium* acme and palynofacies characteristics in the latest Paleocene–earliest Eocene of northeastern India: biotic response to the Paleocene–Eocene thermal maxima (PETM) in low latitude. Journal of The Paleontological Society of India 51, 75–91.
Prebble, J.G., Crouch, E.M., Carter, L., Cortese, G., Bostok, H., Neil, H., 2016. An epanded modern dinoflagellate cyst dataset for the Southwest Pacific and Southern Hemisphere with environmental associations. Marine Micropaleontology 101, 33–48.
Prebble, J.G., Crouch, E.M., Cortese, G., Carter, L., Neil, H., Bostok, H., 2016. Southwest pacific sea surface conditions during Marine Isotope Stage 11 – Results from dinoflagellate cysts. Palaeogeography, Palaeoclimatology, Palaeoecology 446, 19–31.
Prider, J.N., Christophel, D.C., 2000: Distributional ecology of *Gymnostoma australianum* (Casuarinaceae), a putative palaeoendemic of Australian wet tropic forsts. Australian Journal of Botany 48, 427–434.
Pross, J., Schmiedl, G., 2002. Early Oligocene dinoflagellate cysts from the Upper Rhine Graben (SW Germany): paleoenvironmental and paleoclimatic implications. Marine Micropaleontology 45, 1–24.
Raine, J.I., 1984: Outline of a palynological zonation of Cretaceous to Paleogene terrestrial sediments in the West Coast region, South Island. New Zealand Geological Survey report 109. 82 p.
Raine, J.I., Kennedy, E.M., Crouch, E.M., 2009: New Zealand Paleogene vegetation and climate. *In* Crouch, E., Strong, C.P., Hollis, C. (eds.), Climatic and Biotic Events of the Paleogene (CBEP), extended abstracts from an international conference in Wellington, New Zealand. GNS Science Miscellaneous Series 18, 117–122.
Raine, J.I., Beu, A.G., Boyes, A., Campbell, H.J., Cooper, R.A., Crampton, J.S., Crundwell, M., Hollis, C.J., Morgans, H.E.G., Mortimer, N., 2015. New Zealand Geological Timescale NZGT 2015/1. New Zealand Journal of Geology and Geophysics 58, 398–403.
Reay, M., 1993. Geology of the middle part of the Clarence Valley. Institute of Geological and Nuclear Sciences Geological Map 10, 1-144.
Reichart, G.-J., Brinkhuis, H., Huiskamp, F., Zachariasse, W.J., 2004. Hyperstratification following glacial overturning events in the northern Arabian Sea. Paleoceanography 19, PA2013, doi:10.1029/2003PA000900.
Schmitz, B., Pujalte, V., 2007. Abrupt increase in seasonal extreme precipitation at the Paleocene–Eocene boundary. Geology 35, 215–218.
Schneider, L. J., Bralower, T. J., Kump, L. R., 2011. Response of nannoplankton to early Eocene ocean destratification. Palaeoceanography, Palaeoclimatology, Palaeoecology 310, 152–162.
Schouten, S., Hopmans, E.C., Schefuss, E., Sinninghe Damsté, J.S., 2002. Distributional variations in marine crenarchaeotal membrane lipids: a new tool for reconstructing ancient sea water temperatures? Earth and Planetary Science Letters 204, 265-274, doi: 10.1016/S0012-821X(02)00979-2.
Schouten, S., Forster, A., Panato, F., Sinninghe Damsté, J.S., 2007. Towards calibration of the TEX_{86} palaeothermometer for tropical sea surface temperatures in ancient greenhouse worlds. Organic Geochmistry 38, 1537–1546, doi: 10.1016/j.orggeochem.2007.05.014.
Shamrock, J. L., Watkins, D. K., 2012. Eocene calcareous nannofossil biostratigraphy and community structure from Exmouth Plateau, Eastern Indian Ocean (ODP Site 762). Stratigraphy 9. 54 pp.
Shepherd, C. L., 2017. Early to middle Eocene calcareous nannofossils of the SW Pacific: Paleobiogeography and paleoclimate (Unpublished doctoral thesis). Victoria University of Wellington, Wellington, New Zealand. 171 p.
Shepherd, C. L., Kulhanek, D. K., 2016. Eocene nannofossil biostratigraphy of the mid-Waipara River section, Canterbury Basin, New Zealand. Journal of Nannoplankton Research 36, 33–59.
Siesser, W.G., 1993. Calcareous nannoplankton. *In* Lipps, J.H. (ed.), Fossil Prokaryotes and Protists. Blackwell Scientific Publications, 169–201.

Sinninghe Damsté, J.S., Schouten, S., Hopmans, E.C., van Duin, A.C.T., Geenevasen, J., 2002. Crenarchaeol: the characteristic core glycerol dibiphytanyl glycerol tetraether membrane lipid of cosmopolitan pelagic crenarchaeota. Journal of Lipid Research 43, 1641-1651, doi: 10.1194/jlr.M200148-JLR200.
Sinninghe Damsté, J.S., 2016. Spatial heterogeneity of sources of branched tetraethers in shelf systems: The geochemistry of tetraethers in the Berau River delta (Kalimantan, Indonesia). Geochimica et Cosmochimica Acta 186, 13-31.
Slimani, H., Guédé, K. E., Williams, G.L., Asebriy, L., Ahmamou, M., 2016. Campanian to Eocene dinoflagellate biostratigraphy from the Tahar and Sekada sections at Arba Ayacha, western External Rif, Morocco. Review of Palaeobotany and Palynology 228, 26–46.
Slotnick, B.S., Dickens, G.R., Nicolo, M.J., Hollis, C.J., Crampton, J.S., Zachos, J.C., Sluijs, A., 2012. Large-amplitude variations in carbon cycling and terretrial weathering during the Latest Paleocene and Earliest Eocene: the record at Mead Stream, New Zealand. The Journal of Geology 120, 487–505.
Slotnick, B.S., Dickens, G.R., Hollis, C.J., Crampton, J.S., Strong, C.P., Phillips, A., 2015. The onset of the Early Eocene Climatic Optimum at Branch Stream, Clarence River valley, New Zealand. New Zealand Journal of Geology and Geophysics 58, 262–280.
Sluijs, A., Pross, J., Brinkhuis, H., 2005. From greenhouse to icehouse; organic-walled dinoflagellate cysts as paleoenvironmental indicators in the Paleogene. Earth-Science Reviews 68, 281–315.
Sluijs, A., Brinkhuis, H., 2009. A dynamic climate and ecosystem state during the Paleocene–Eocene Thermal Maximum: inferences from dinoflagellate cyst assemblages on the New Jersey Shelf. Biogeosciences 6, 1755–1781.
Steane, D.A., Wilson, K.L., Hill, R.S., 2003. Using *mat*K sequence data to unravel the phyologeny of Casuarinaceae. Molecular Phylogenetics and Evolution 28, 47–59.
Taylor, K.W.R., Huber, M., Hollis, C.J., Hernandez-Sanchez, M.T., Pancost, R.D., 2013. Re-evaluating modern and Palaeogene GDGT distributions: Implications for SST reconstructions. Global and Planetary Change 108, 158-174, doi: 10.1016/j.gloplacha.2013.06.011.
Taylor, K.W.R., Willumsen, P.S., Hollis, C.J., Pancost, R.D., 2018. South pacific evidence for the long-term climate impact of the Cretaceous/Paleogene boundary event. Earth-Science Reviews 179, 287–302.
Tierney, J.E., Tingley, M.P., 2014. A Bayesian, spatially-varying calibration model for the TEX_{86} proxy. Geochimica et Cosmochimica Acta 127, 83-106, doi: 10.1016/j.gca.2013.11.026.
Tierney, J.E., Tingley, M.P., 2015. A TEX_{86} surface sediment database and extended Bayesian calibration. Scientific Data 2, 150029, doi: 10.1038/sdata.2015.29.
Tierney, J.E., Sinninghe Damsté J., S., Pancost, R.D., Sluijs, A., Zachos, J.C., 2017. Eocene temperature gradients. Nature Geoscience 10, 538-539.
Trommer, G., Siccha, M., van der Meer, M.T.J., Schouten, S., Sinninghe Damsté, J.S., Schulz, H., Hemleben, C., et al., 2009. Distribution of Crenarchaeota tetraether membrane lipids in surface sediments from the Red Sea. Organic Geochemistry 40, 724-731, doi: 10.1016/j.orggeochem.2009.03.001.
Van Hinsbergen, D., de Groot, L., van Schaik, J., Spakman, W., Bijl, P., Sluijs, A., Langereis, C., Brinkhuis, H., 2015. A Paleolatitude Calculator for Paleoclimate Studies, PLOS ONE, 10, 10.1371/journal. pone.0126946.
Villa, G., Persico, D., 2006. Late Oligocene climatic changes: Evidence from calcareous nannofossils at Kerguelen Plateau Site 748 (Southern Ocean). Palaeogeography, Palaeoclimatology, Palaeoecology 231, 110–119, doi: 10.1016/j.palaeo.2005.07.028.
Villa, G., Fioroni, C., Pea, L., Bohaty, S., Persico, D., 2008. Middle Eocene–late Oligocene climate variability: Calcareous nannofossil response at Kerguelen Plateau, Site 748. Marine Micropaleontology 69, 173–192, doi: 10.1016/j.marmicro.2008.07.006.
Wei, W., Wise, S. W., 1990. Biogeographic gradients of middle Eocene–Oligocene calcareous nannoplankton in the South Atlantic Ocean. Palaeogeography, Palaeoclimatology, Palaeoecology 79, 29–61, doi: 10.1016/0031-0182(90)90104-F.
Weijers, J.W.H., Schouten, S., Hopmans, E.C., Geenevasen, J.A.J., David, O.R.P., Coleman, J.M., Pancost, R.D., et al., 2006. Membrane lipids of mesophilic anaerobic bacteria thriving in peats have typical archaeal traits. Environmental Microbiology 8, 648-657, doi: 10.1111/j.1462-2920.2005.00941.x.
Weijers, J.W.H., Schouten, S., van den Donker, J.C., Hopmans, E.C., Sinninghe Damsté, J.S., 2007. Environmental controls on bacterial tetraether membrane lipid distribution in soils. Geochimica et Cosmochimica Acta 71, 703-713, doi: 10.1016/j.gca.2006.10.003.
Westerhold, T., Röhl, U., 2009. High resolution cyclostratigraphy of the early Eocene – new insights into the origin of the Cenozoic cooling trend. Climate of the Past 5, 309–327.
Westerhold, T., Röhl, U., Laskar, J., 2012. Time scale controversy: Accurate orbital calibration of the early Paleogene. Geochemistry, Geophysics, Geosystems 13, Q06015, doi:10.1029/2012GC004096.

1407 Westerhold, T., Röhl, U., Frederichs, T., Agnini, C., Raffi, I., Zachos, J.C., Wilkins, R.H., 2017. Astronomical
1408 calibration of the Ypresian Time Scale: Implications for seafloor spreading rates and the chaotic behaviour
1409 of the solar system? Climate of the Past 13, 1129–1152.
1410 Westerhold, T., Röhl, U., Donner, B., Zachos, J.C., 2018. Global extent of the Early Eocene hyperthermal
1411 events – a new Pacific benthic foraminiferal isotope record from Shatsky Rise (ODP site 1209).
1412 Paleoceanography and Paleoclimatology 33, 626–642, doi:10.1029/2017PA003306.
1413 Wilson, G.J., 1984. New Zealand Late Jurassic to Eocene dinoflagellate biostratigraphy – a summary.
1414 Newsletters on Stratigraphy 13, 104–117.
1415 Wilson, G.J., 1988. Paleocene and Eocene dinoflagellate cysts from Waipawa, Hawkes Bay, New Zealand. New
1416 Zealand Geological Survey Paleontological Bulletin 57. 96p.
1417 Wrenn, J.H., Beckman, S.W., 1982. Maceral, total organic carbon and palynological analyses of Ross Ice Shelf
1418 Project Site J9 cores. Science 216, 187–189, doi:10.1126/science.216.4542.187.
1419 Zachos, J.C., Pagani, M., Sloan, L., Thomas, E., Billups, K., 2001. Trends, rhythms, and aberrations in global
1420 climate 65 Ma to present. Science 292, 686–693.
1421 Zachos, J.C., Schouten, S., Bohart, S., Quattlebaum, T., Sluijs, A., Brinkhuis, H., Gibbs, S., Bralower, T., 2006.
1422 Extreme warming of mid-latitude coastal ocean during the Paleocene–Eocene Thermal Maximum:
1423 Inferences from TEX86 and isotope data. Geology 34, 737–740.
1424 Zachos, J.C., Dickens, G.R., Zeebe, R.E., 2008. An early Cenozoic perspective on greenhouse warming and
1425 carbon-cycle dynamics. Nature 45, 279–283.
1426 Zhang, Y.G., Zhang, C.L., Liu, X.-L., Li, L., Hinrichs, K., Noakes, J.E., 2011. Methane Index: A tetraether
1427 archaeal lipid biomarker indicator for detecting the instability of marine gas hydrates. Earth and Planetary
1428 Science Letters 307, 525–534.
1429 Zonneveld, K.A.F., Marret, F., Versteegh, G., Bogus, K., Bonnet, S., Bouimetarhan, I., Crouch, E.M., de
1430 Vernal, A., et al., 2013. Atlas of modern dinoflagellate cyst distribution based on 2045 data points. Review
1431 of Palaeobotany and Palynology 191, 1–197.
1432

Figure 1

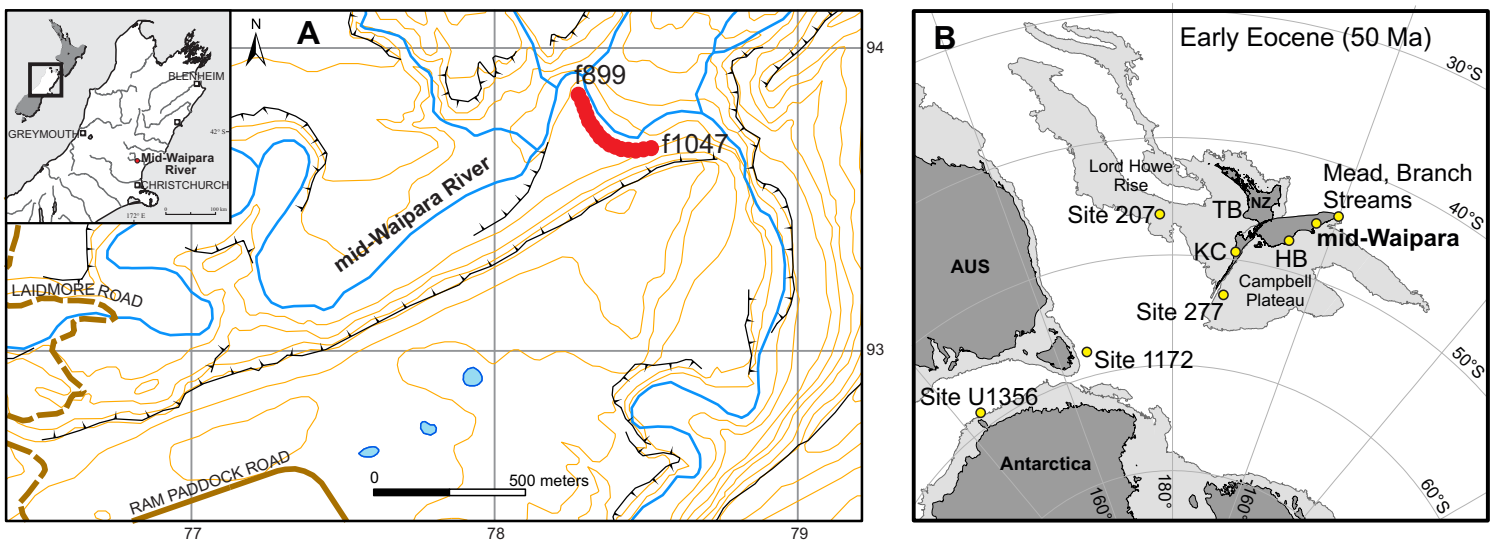
A
N
BLENHEIM
GREYMOUTH
Mid-Waipara River
CHRISTCHURCH
f899
f1047
mid-Waipara River
LAIDMORE ROAD
RAM PADDOCK ROAD
0
500 meters
94
93
77
78
79
B
Early Eocene (50 Ma)
30°S
40°S
50°S
60°S
Lord Howe Rise
Site 207
TB
NZ
Mead, Branch Streams
mid-Waipara
KC
HB
Campbell Plateau
Site 277
AUS
Site 1172
Site U1356
Antarctica
160°
180°
160°

Figure 2

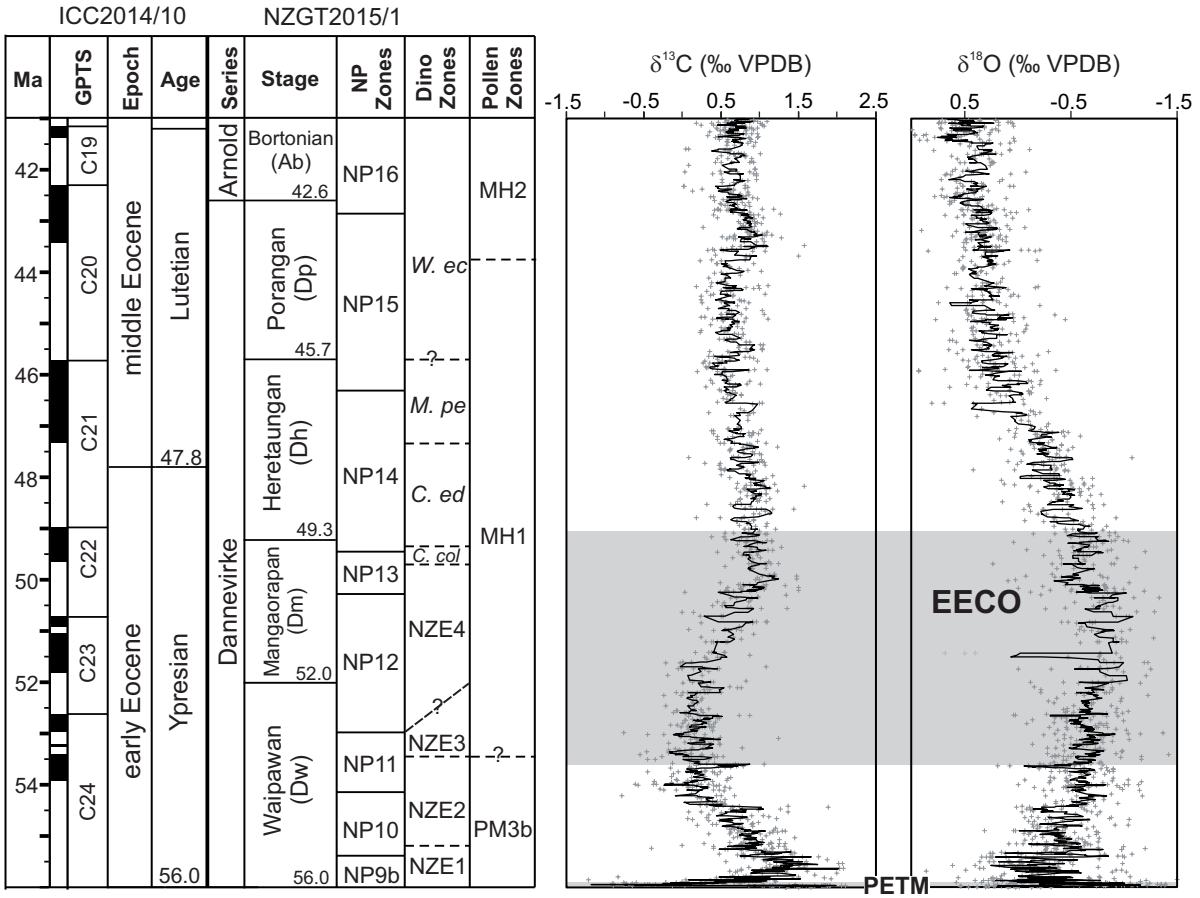
ICC2014/10
NZGT2015/1
Ma
GPTS
Epoch
Age
Series
Stage
NP Zones
Dino Zones
Pollen Zones
42
44
46
48
50
52
54
C19
C20
C21
C22
C23
C24
middle Eocene
early Eocene
Lutetian
Ypresian
47.8
56.0
Arnold
Dannevirke
Bortonian (Ab)
42.6
Porangan (Dp)
45.7
Heretaungan (Dh)
49.3
Mangaorapan (Dm)
52.0
Waipawan (Dw)
56.0
NP16
NP15
NP14
NP13
NP12
NP11
NP10
NP9b
W. ec
?
M. pe
C. ed
C. col
NZE4
?
NZE3
?
NZE2
NZE1
MH2
MH1
PM3b
δ13C (‰ VPDB)
-1.5
-0.5
0.5
1.5
2.5
δ18O (‰ VPDB)
0.5
-0.5
-1.5
EECO
PETM

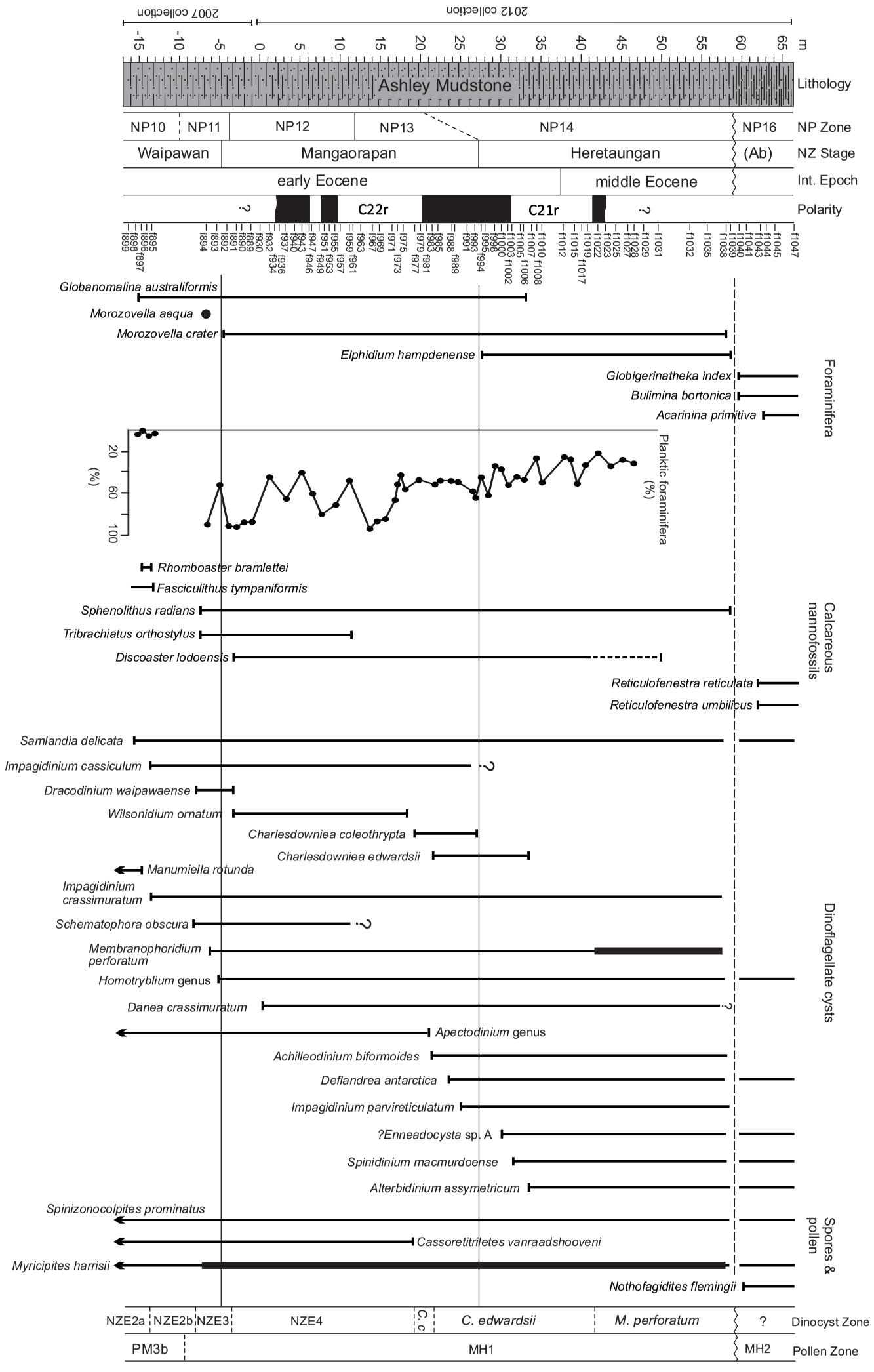
2007 collection
2012 collection
m
Lithology
Ashley Mudstone
NP Zone
NP10
NP11
NP12
NP13
NP14
NP16
NZ Stage
Waipawan
Mangaorapan
Heretaungan
(Ab)
Int. Epoch
early Eocene
middle Eocene
Polarity
C22r
C21r
Globanomalina australiformis
Morozovella aequa
Morozovella crater
Elphidium hampdenense
Globigerinatheka index
Bulimina bortonica
Acarinina primitiva
Foraminifera
Planktic foraminifera (%)
Rhomboaster bramlettei
Fasciculithus tympaniformis
Sphenolithus radians
Tribrachiatus orthostylus
Discoaster lodoensis
Reticulofenestra reticulata
Reticulofenestra umbilicus
Calcareous nannofossils
Samlandia delicata
Impagidinium cassiculum
Dracodinium waipawaense
Wilsonidium ornatum
Charlesdowniea coleothrypta
Charlesdowniea edwardsii
Manumiella rotunda
Impagidinium crassimuratum
Schematophora obscura
Membranophoridium perforatum
Homotryblium genus
Danea crassimuratum
Apectodinium genus
Achilleodinium biformoides
Deflandrea antarctica
Impagidinium parvireticulatum
?Enneadocysta sp. A
Spinidinium macmurdoense
Alterbidinium assymetricum
Dinoflagellate cysts
Spinizonocolpites prominatus
Cassoretitriletes vanraadshooveni
Myricipites harrisii
Nothofagidites flemingii
Spores & pollen
NZE2a
NZE2b
NZE3
NZE4
C. c.
C. edwardsii
M. perforatum
Dinocyst Zone
PM3b
MH1
MH2
Pollen Zone

Figure 3

Figure 4

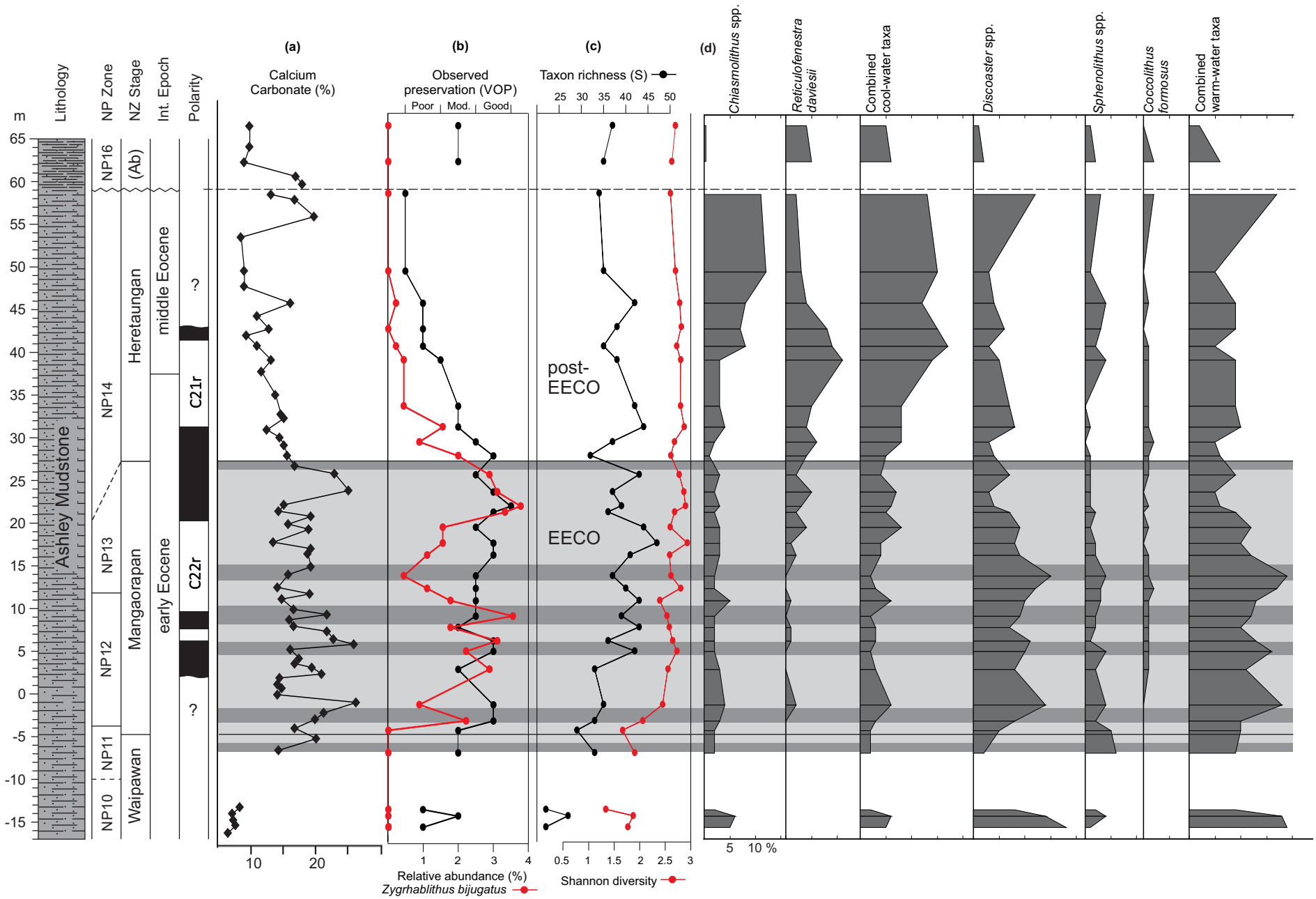
Lithology
NP Zone
NZ Stage
Int. Epoch
Polarity
m
Ashley Mudstone
NP16
NP14
NP13
NP12
NP11
NP10
(Ab)
Heretaungan
Mangaorapan
Waipawan
middle Eocene
early Eocene
C21r
C22r
?
?
(a)
Calcium Carbonate (%)
(b)
Observed preservation (VOP)
Poor
Mod.
Good
(c)
Taxon richness (S)
post-EECO
EECO
(d)
Chiasmolithus spp.
Reticulofenestra daviesii
Combined cool-water taxa
Discoaster spp.
Sphenolithus spp.
Coccolithus formosus
Combined warm-water taxa
Relative abundance (%)
Zygrhablithus bijugatus
Shannon diversity
5 10 %

Figure 5

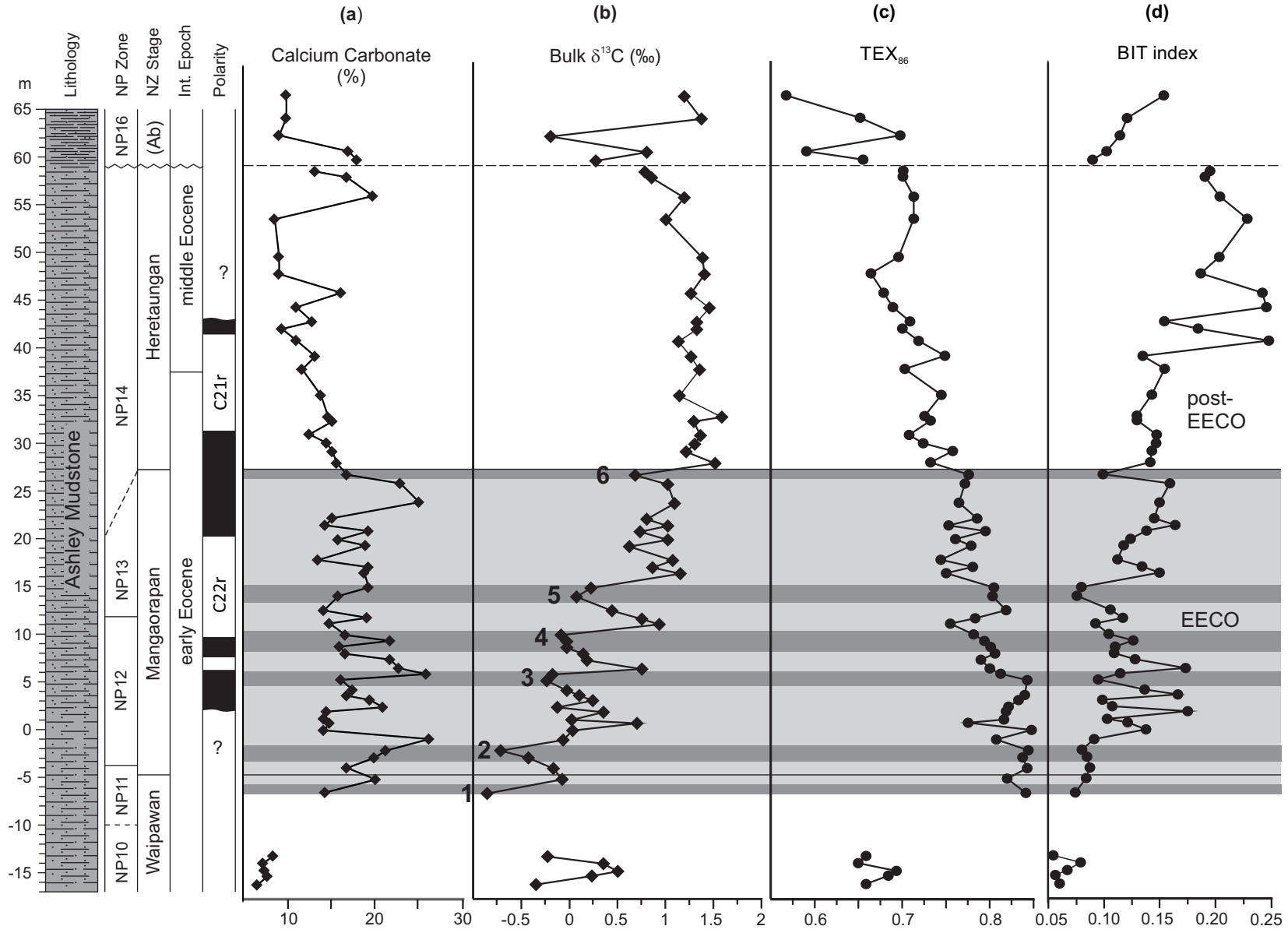
(a)
Calcium Carbonate (%)
(b)
Bulk δ13C (‰)
(c)
TEX86
(d)
BIT index
Lithology
NP Zone
NZ Stage
Int. Epoch
Polarity
m
Ashley Mudstone
NP16
NP14
NP13
NP12
NP11
NP10
(Ab)
Heretaungan
Mangaorapan
Waipawan
middle Eocene
early Eocene
C21r
C22r
?
?
post-EECO
EECO
1
2
3
4
5
6
65
60
55
50
45
40
35
30
25
20
15
10
5
0
-5
-10
-15
10
20
30
-0.5
0
0.5
1
1.5
2
0.6
0.7
0.8
0.05
0.10
0.15
0.20
0.25

Figure 6

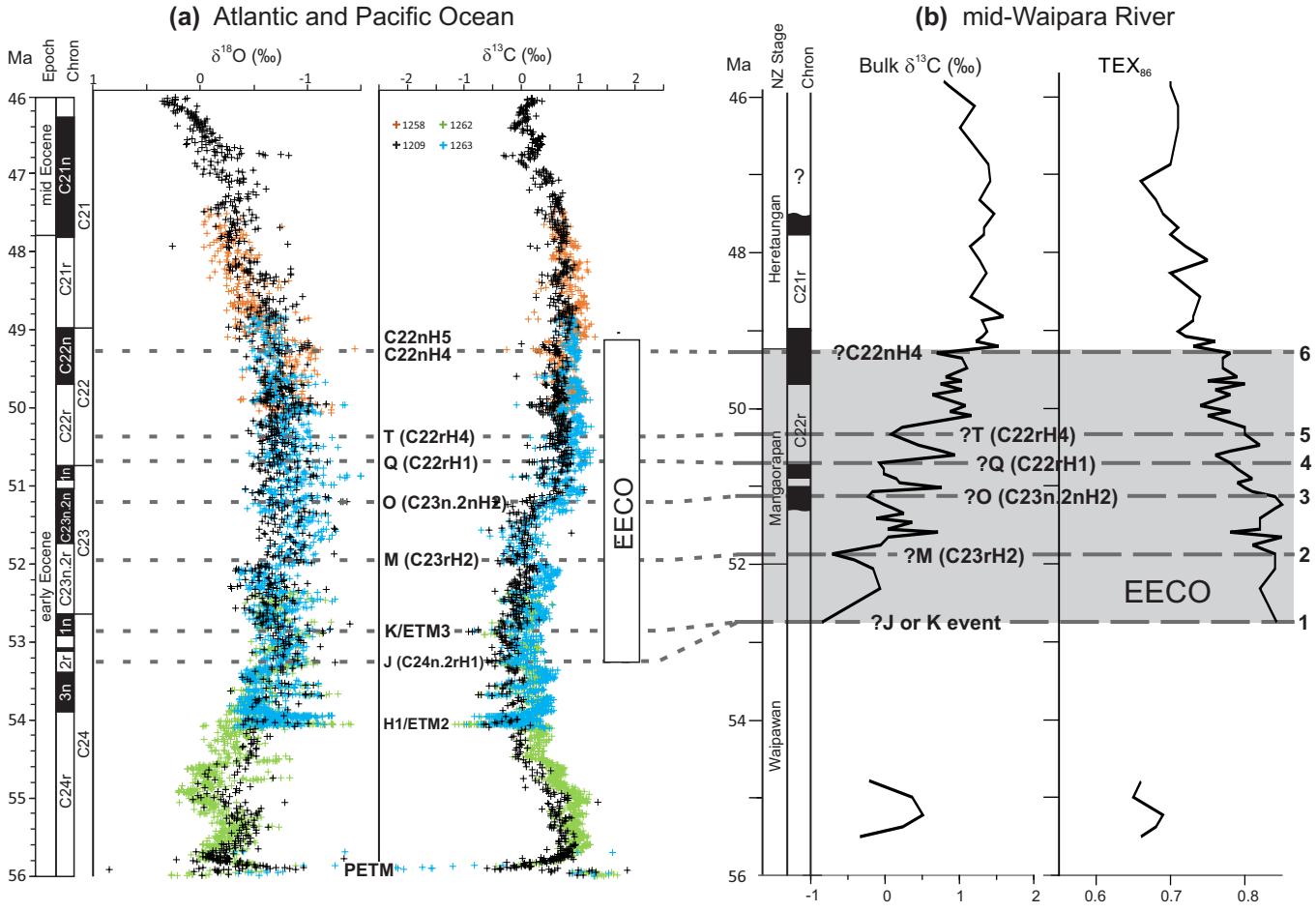
(a) Atlantic and Pacific Ocean
(b) mid-Waipara River
Ma
Epoch
Chron
δ18O (‰)
δ13C (‰)
1258
1262
1209
1263
mid Eocene
early Eocene
C21n
C21r
C22n
C22r
C23n.2n
C23n.2r
1n
2r
3n
C24r
C21
C22
C23
C24
C22nH5
C22nH4
T (C22rH4)
Q (C22rH1)
O (C23n.2nH2)
M (C23rH2)
K/ETM3
J (C24n.2rH1)
H1/ETM2
PETM
EECO
NZ Stage
Heretaungan
Mangaorapan
Waipawan
Bulk δ13C (‰)
TEX86
?C22nH4
?T (C22rH4)
?Q (C22rH1)
?O (C23n.2nH2)
?M (C23rH2)
?J or K event
EECO
6
5
4
3
2
1

Figure 7

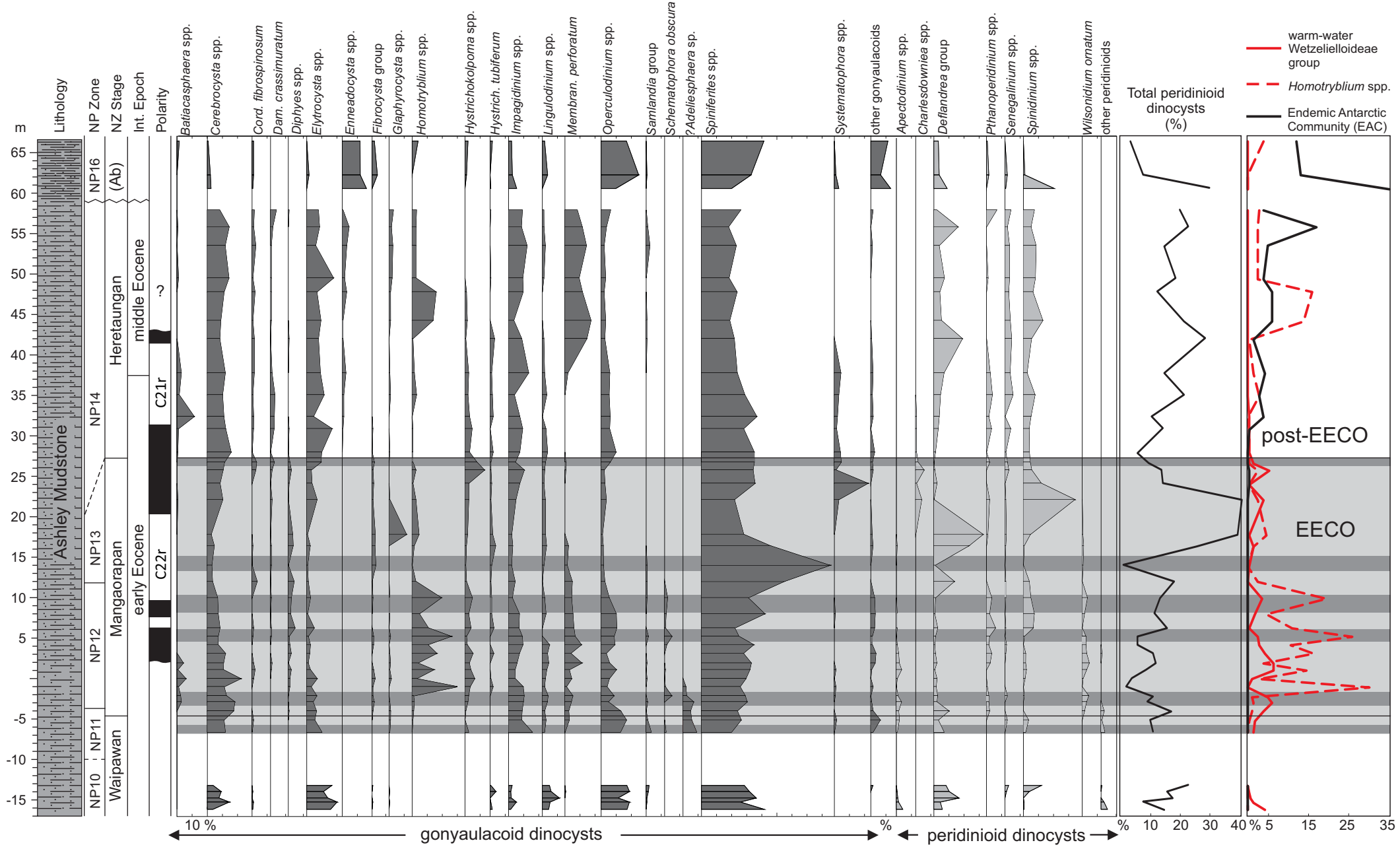
m
Lithology
NP Zone
NZ Stage
Int. Epoch
Polarity
Ashley Mudstone
NP16
NP14
NP13
NP12
NP11
(Ab)
Heretaungan
Mangaorapan
Waipawan
middle Eocene
early Eocene
?
C21r
C22r
Batiacasphaera spp.
Cerebrocysta spp.
Cord. fibrospinosum
Dam. crassimuratum
Diphyes spp.
Elytrocysta spp.
Enneadocysta spp.
Fibrocysta group
Glaphyrocysta spp.
Homotryblium spp.
Hystrichokolpoma spp.
Hystrich. tubiferum
Impagidinium spp.
Lingulodinium spp.
Membran. perforatum
Operculodinium spp.
Samlandia group
Schematophora obscura
?Adeliesphaera sp.
Spiniferites spp.
Systematophora spp.
other gonyaulacoids
Apectodinium spp.
Charlesdowniea spp.
Deflandrea group
Pthanoperidinium spp.
Senegalinium spp.
Spinidinium spp.
Wilsonidium ornatum
other peridinioids
Total peridinioid dinocysts (%)
warm-water Wetzelielloideae group
Homotryblium spp.
Endemic Antarctic Community (EAC)
post-EECO
EECO
10 %
gonyaulacoid dinocysts
%
peridinioid dinocysts
%
10 20 30 40
% 5 15 25 35

Figure 8

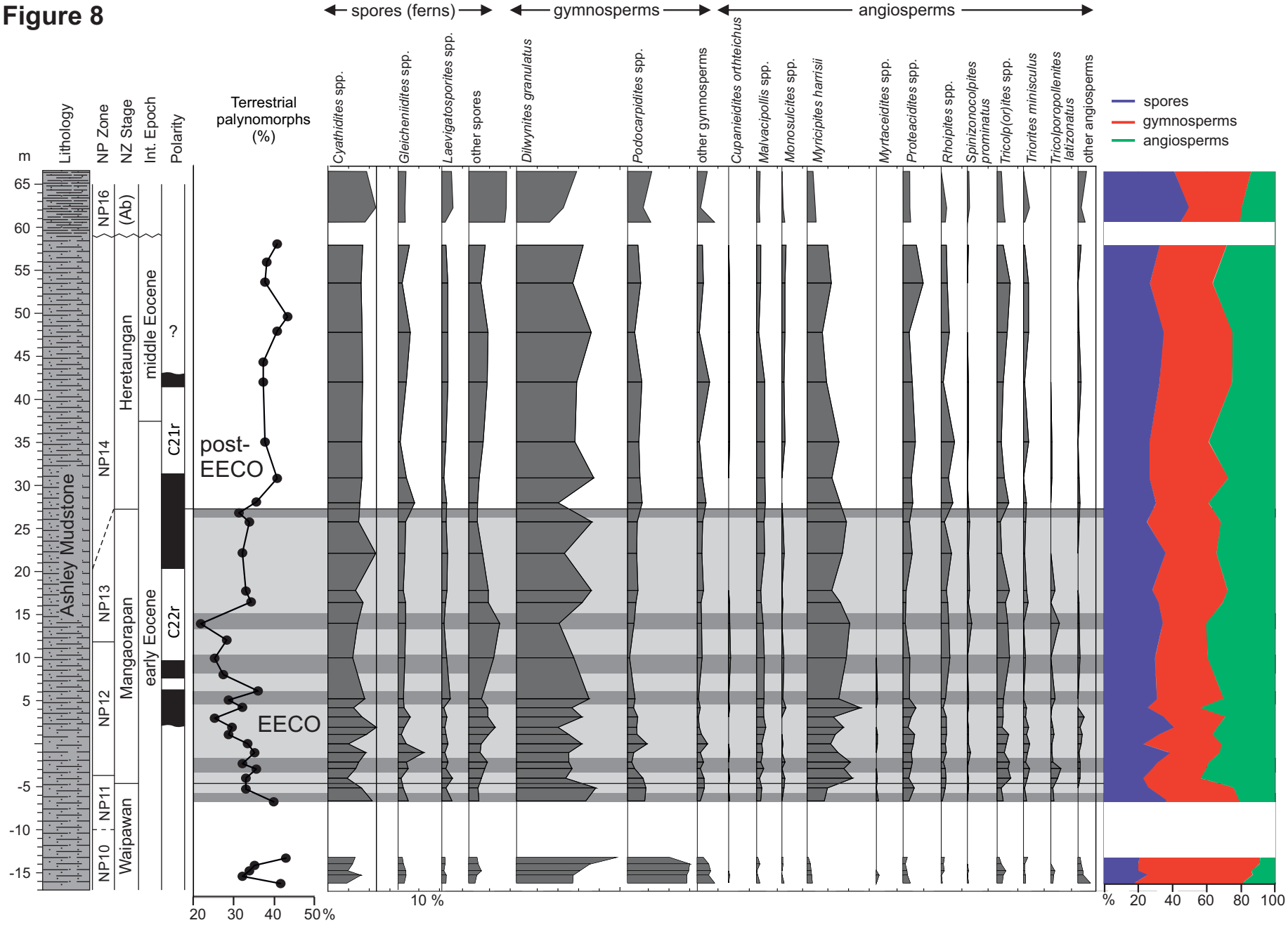
spores (ferns)
gymnosperms
angiosperms
Lithology
NP Zone
NZ Stage
Int. Epoch
Polarity
Terrestrial palynomorphs (%)
Cyathidites spp.
Gleicheniidites spp.
Laevigatosporites spp.
other spores
Dilwynites granulatus
Podocarpidites spp.
other gymnosperms
Cupanieidites orthteichus
Malvacipollis spp.
Monosulcites spp.
Myricipites harrisii
Myrtaceidites spp.
Proteacidites spp.
Rhoipites spp.
Spinizonocolpites prominatus
Tricolp(or)ites spp.
Triorites miniusculus
Tricolporopollenites latizonatus
other angiosperms
spores
gymnosperms
angiosperms
m
Ashley Mudstone
NP16
(Ab)
NP14
NP13
NP12
NP11
NP10
Heretaungan
Mangaorapan
Waipawan
middle Eocene
early Eocene
C21r
C22r
?
post-EECO
EECO
20 30 40 50 %
10 %
% 20 40 60 80 100

Figure 9

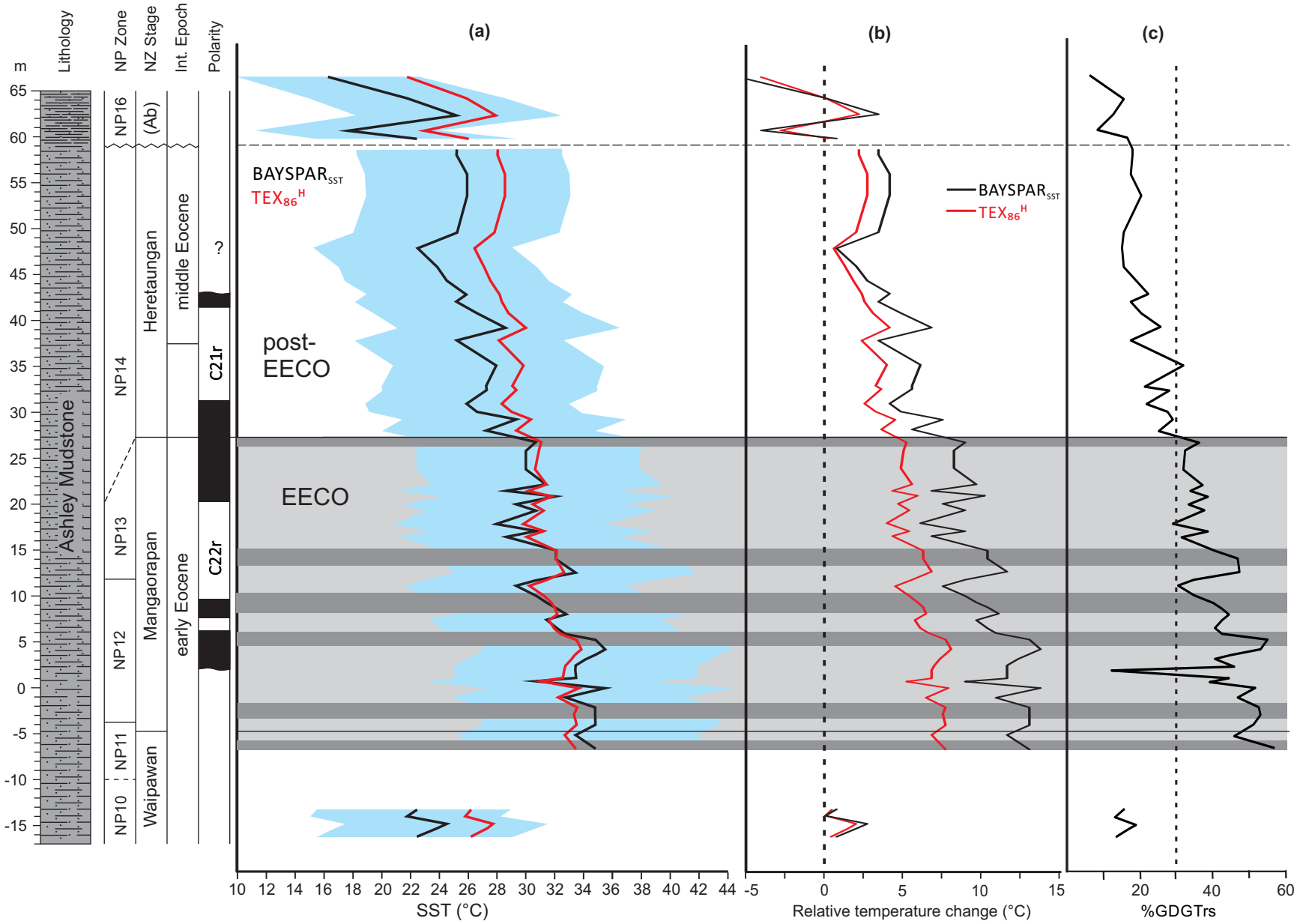
m
Lithology
NP Zone
NZ Stage
Int. Epoch
Polarity
Ashley Mudstone
NP16
NP14
NP13
NP12
NP11
NP10
(Ab)
Heretaungan
Mangaorapan
Waipawan
middle Eocene
early Eocene
?
C21r
C22r
(a)
(b)
(c)
BAYSPAR$_{SST}$
TEX$_{86}^{H}$
post-
EECO
EECO
SST (°C)
Relative temperature change (°C)
%GDGTrs

Figure 10

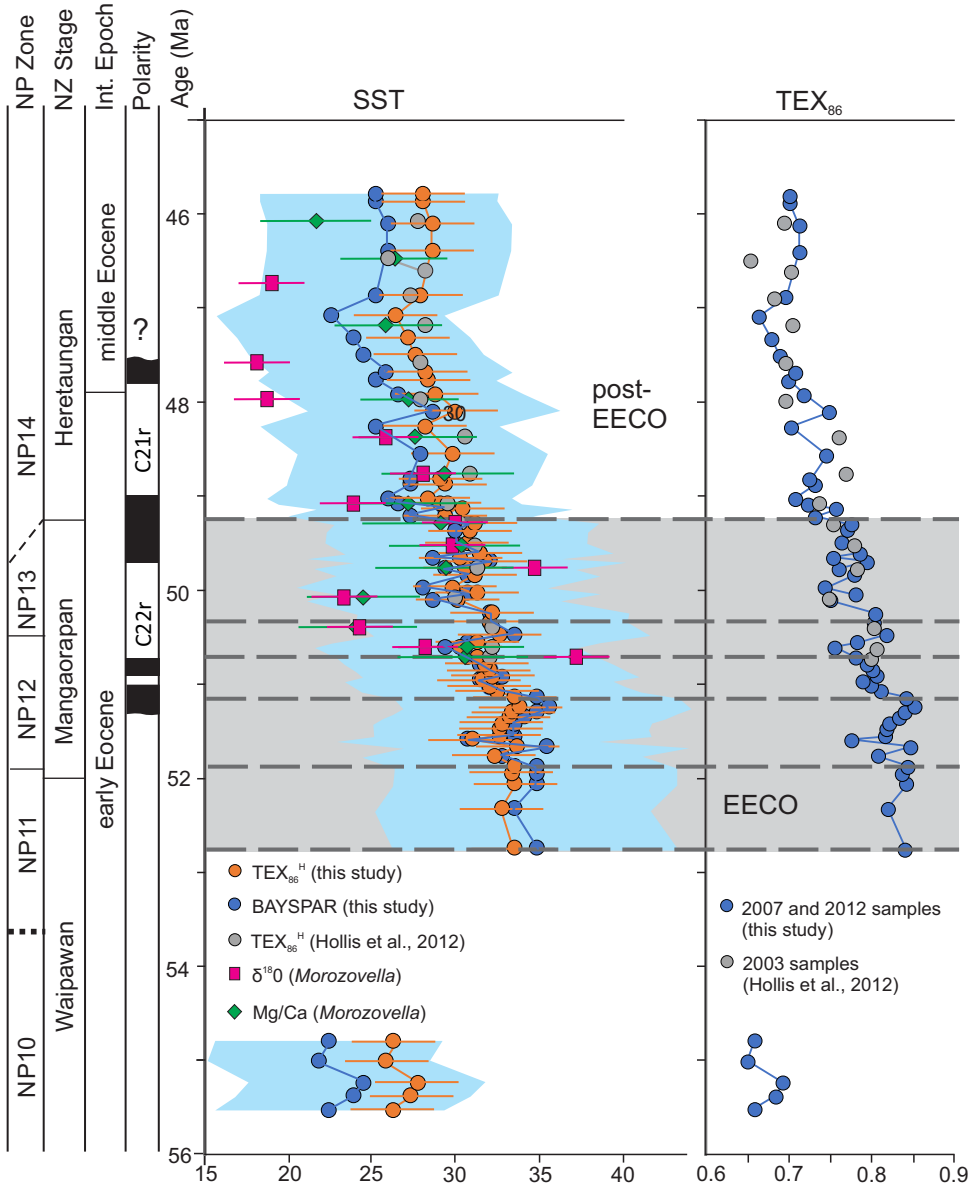
NP Zone
NZ Stage
Int. Epoch
Polarity
Age (Ma)
SST
TEX86
NP14
NP13
NP12
NP11
NP10
Heretaungan
Mangaorapan
Waipawan
middle Eocene
early Eocene
?
C21r
C22r
post-
EECO
EECO
30
46
48
50
52
54
56
15
20
25
30
35
40
0.6
0.7
0.8
0.9
TEX86H (this study)
BAYSPAR (this study)
TEX86H (Hollis et al., 2012)
δ18O (Morozovella)
Mg/Ca (Morozovella)
2007 and 2012 samples
(this study)
2003 samples
(Hollis et al., 2012)

Figure 11

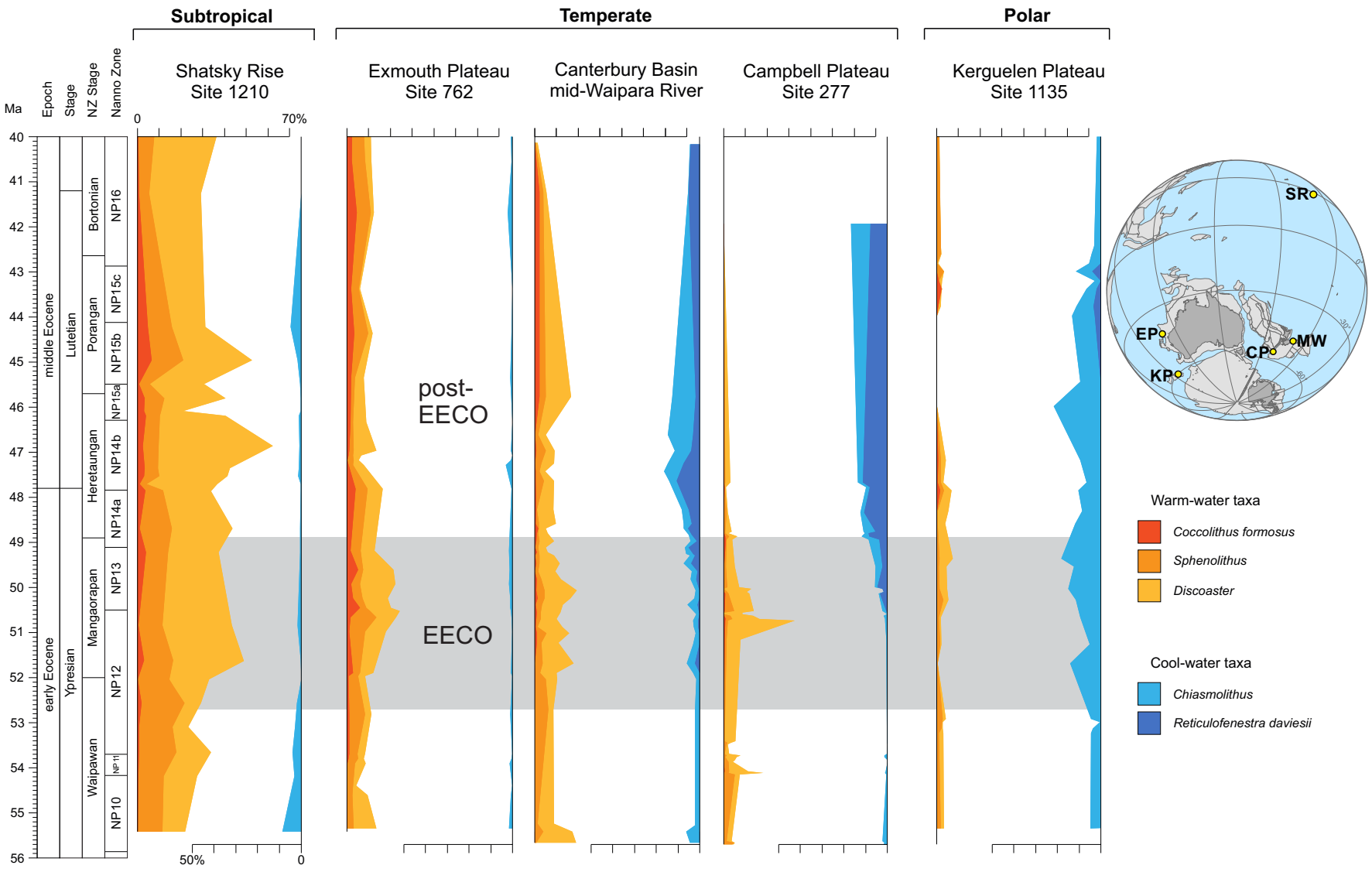
Subtropical
Temperate
Polar
Shatsky Rise
Site 1210
Exmouth Plateau
Site 762
Canterbury Basin
mid-Waipara River
Campbell Plateau
Site 277
Kerguelen Plateau
Site 1135
Ma
Epoch
Stage
NZ Stage
Nanno Zone
0
70%
50%
0
post-
EECO
EECO
middle Eocene
early Eocene
Lutetian
Ypresian
Bortonian
Porangan
Heretaungan
Mangaorapan
Waipawan
NP16
NP15c
NP15b
NP15a
NP14b
NP14a
NP13
NP12
NP11
NP10
SR
EP
CP
MW
KP
Warm-water taxa
Coccolithus formosus
Sphenolithus
Discoaster
Cool-water taxa
Chiasmolithus
Reticulofenestra daviesii

Figure 12

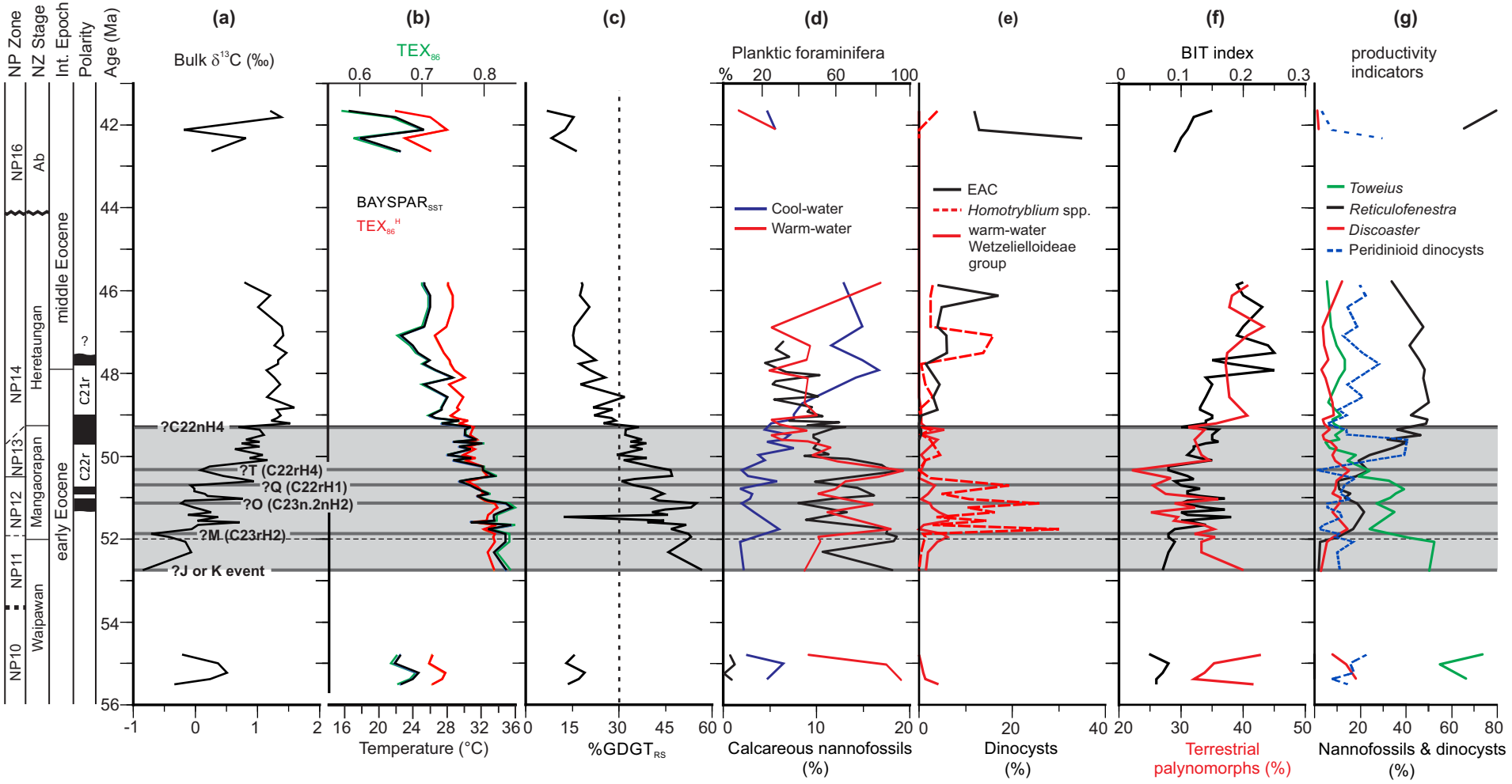
NP Zone
NZ Stage
Int. Epoch
Polarity
Age (Ma)
NP16
NP14
NP13
NP12
NP11
NP10
Ab
Heretaungan
Mangaorapan
Waipawan
middle Eocene
early Eocene
C21r
C22r
?
?C22nH4
?T (C22rH4)
?Q (C22rH1)
?O (C23n.2nH2)
?M (C23rH2)
?J or K event
(a)
Bulk δ13C (‰)
(b)
TEX86
BAYSPARSST
TEX86H
Temperature (°C)
(c)
%GDGTRS
(d)
Planktic foraminifera
Cool-water
Warm-water
Calcareous nannofossils (%)
(e)
EAC
Homotryblium spp.
warm-water Wetzelielloideae group
Dinocysts (%)
(f)
BIT index
Terrestrial palynomorphs (%)
(g)
productivity indicators
Toweius
Reticulofenestra
Discoaster
Peridinioid dinocysts
Nannofossils & dinocysts (%)